

1 **Improving the global applicability of the RUSLE model –**
2 **Adjustment of the topographical and rainfall erosivity factors**

3
4 V. Naipal¹, C. Reick¹, J. Pongratz¹, K. Van Oost²

5 [1] {Max Planck Institute for Meteorology, Hamburg 20146, Germany}

6 [2] {Université catholique de Louvain, TECLIM – Georges Lemaître Centre for Earth and
7 Climate Research, Louvain-la-Neuve, Belgium}

8 Received: 12 February 2015 – Accepted: 6 March 2015 – Published: 19 March 2015

9 Correspondence to: V. Naipal (victoria.naipal@mpimet.mpg.de)

10 Published by Copernicus Publications on behalf of the European Geosciences Union

11

12 **Abstract**

13 Large uncertainties exist in estimated rates and the extent of soil erosion by surface runoff on a
14 global scale, and this limits our understanding of the global impact that soil erosion might have
15 on agriculture and climate. The Revised Universal Soil Loss Equation (RUSLE) model, due to its
16 simple structure and empirical basis, is a frequently used tool in estimating average annual soil
17 erosion rates at regional to global scales. However, large spatial scale applications often rely on
18 coarse data input, which is not compatible with the local scale at which the model is
19 parameterized. This study aimed at providing the first steps in improving the global applicability
20 of the RUSLE model in order to derive more accurate global soil erosion rates.

21 We adjusted the topographical and rainfall erosivity factors of the RUSLE model and compared
22 the resulting soil erosion rates to extensive empirical databases on soil erosion from the USA and
23 Europe. Adjusting the topographical factor required scaling of slope according to the fractal
24 method, which resulted in improved topographical detail in a coarse resolution global digital
25 elevation model.

26 Applying the linear multiple regression method to adjust rainfall erosivity for various climate
27 zones resulted in values that compared well to high resolution erosivity data for different regions.
28 However, this method needs to be extended to tropical climates, for which erosivity is biased due
29 to the lack of high resolution erosivity data.

30 After applying the adjusted and the unadjusted versions of the RUSLE model on a global scale
31 we find that the adjusted RUSLE model not only shows a global higher mean soil erosion rate
32 but also more variability in the soil erosion rates. Comparison to empirical datasets of the USA
33 and Europe shows that the adjusted RUSLE model is able to decrease the very high erosion rates
34 in hilly regions that are observed in the unadjusted RUSLE model results. Although there are still
35 some regional differences with the empirical databases, the results indicate that the methods used
36 here seem to be a promising tool in improving the applicability of the RUSLE model on a coarse
37 resolution on global scale.

38

39 **1 Introduction**

40 For the last centuries to millennia soil erosion by surface runoff is being accelerated globally due
41 to human activities, such as deforestation and agricultural practices (Bork and Lang, 2003).
42 Accelerated soil erosion is a process that triggers land degradation in the form of nutrient loss, a
43 decrease in the effective root depth, water imbalance in the root zone and finally also
44 productivity reduction (Yang et al., 2003). It is widely recognized that soil erosion is a major
45 threat to sustainable agriculture and food production across the globe for many decades. These
46 effects of soil erosion are currently exacerbated by the global population growth and climatic
47 changes. Organizations such as the United Nations Convention to Combat Desertification
48 (UNCCD) try to address this problem by stating a new goal for Rio +20 of zero land degradation
49 (UNCCD, 2012).

50 Another aspect underpinning the relevance of soil erosion on the global scale is the effect of soil
51 erosion on the global nutrient cycles. Recently, the biogeochemical components of Earth System
52 Models (ESMs) became increasingly important in predicting the global future climate (Thornton
53 et al., 2007; Goll et al., 2012). Not only the global carbon cycle but also other nutrient cycles
54 such as the nitrogen (N) and phosphorous (P) cycles cannot be neglected in ESMs anymore (Goll
55 et al., 2012; Gruber and Galloway, 2008; Reich et al., 2006). Soil erosion may have a significant

56 impact on these nutrient cycles through lateral fluxes of sediment, but the impact on the global
57 scale is still largely unknown. For example, Quinton et al. (2010) showed that erosion can
58 significantly alter the nutrient and carbon cycling and result in lateral fluxes of nutrients that are
59 similar in magnitude as fluxes induced by fertilizer application and crop removal. Regnier et al.
60 (2013) looked at the effect of human induced lateral fluxes of carbon from land to ocean and
61 concluded that human perturbations, which include soil erosion, may have enhanced the carbon
62 export from soils to inland waters.

63 In general, the effect of soil erosion on the global carbon cycle has received considerable
64 attention after the pioneering work of Stallard (1998), who proposed that global soil erosion can
65 result in sequestration of carbon by soils. After his work, the effect of soil erosion on the carbon
66 cycle has been studied extensively, but there remains a large uncertainty in the effect of soil
67 erosion on the carbon cycle. For example, several recent global assessments of the influence of
68 soil erosion on the carbon cycle indicate a large uncertainty with a range from a source of 0.37 to
69 1 Pg C year⁻¹ to a net uptake or sink of 0.56 to 1 Pg C year⁻¹ (van Oost et al., 2007). Thus, in
70 order to better constrain the global carbon budget and to identify optimal management strategies
71 for land use, it is essential to have accurate estimates of soil erosion and its variability on a
72 global scale.

73 Currently, however, there exists a large uncertainty in the global soil erosion rates as can be seen
74 from recent studies that show rates between 20 and 200 Pg y⁻¹ (Doetterl et al., 2012). This
75 indicates that modelling soil erosion on a global scale is still a difficult task due to the very high
76 spatial and temporal variability of soil erosion. Different approaches were previously applied to
77 estimate soil erosion on a large or global scale. Most of these approaches are based on
78 extrapolated data from agricultural plots, sediment yield or extrapolated river sediment estimates
79 (Milliman and Syvitski, 1992, Stallard, 1998, Lal, 2003, Hooke, 2000, Pimentel et al., 1995,
80 Wilkinson and McElroy, 2007). An alternative approach is based on the use of soil erosion
81 models. One of the most applied models to estimate soil erosion on a large spatial scale is the
82 semi-empirical/process-based Revised Universal Soil Loss Equation (RUSLE) model (Renard et
83 al., 1997). This model stems from the original Universal Soil Loss Equation (USLE) model
84 developed by USDA (USA Department of Agriculture), which is based on a large set of
85 experiments on soil loss due to water erosion from agricultural plots in the United States (USA).
86 These experiments covered a large variety of agricultural practices, soil types and climatic

87 conditions, making it a potentially suitable tool on a regional to global scale. The RUSLE model
88 predicts the average annual soil erosion rates by rainfall and is formulated as a product of a
89 rainfall erosivity factor (R), a slope steepness factor (S), a slope length factor (L), a soil
90 erodibility factor (K), a crop cover factor (C) and a support practice factor (P). The RUSLE
91 model was first applied on a global scale by Yang et al. (2003) and Ito (2007) for estimating the
92 global soil erosion potential and various limitations related to applying the RUSLE model on the
93 global scale. Firstly, the model is originally developed to be applicable on the agricultural plot
94 scale, which is not compatible with the coarse spatial scale of global datasets on soil erosion
95 influencing factors such as precipitation, elevation, land-use and soil characteristics. Secondly,
96 the RUSLE and USLE models were parameterized for environmental conditions of the United
97 States (USA), and are thus not directly applicable to other areas in the world. Thirdly, only sheet
98 and rill erosion are considered, and finally the RUSLE model does not contain sediment
99 deposition and sediment transport terms, which are closely linked to soil erosion.

100 The RUSLE model is to our knowledge one of the few erosion models that has the potential to be
101 applied on a global scale due to its simple structure and empirical basis. Therefore it is of key
102 importance to address the above mentioned limitations first.

103 To address the first two limitations, Van Oost et al. (2007) presented in their work a modified
104 version of the USLE model for application on agricultural areas on a global scale. They based
105 their model on large-scale experimental soil erosion data from the USA (National Resource
106 Inventory, NRI database, USDA, 2000) and Europe, by deriving reference factors for soil
107 erosion and for certain RUSLE parameters. They also introduced a procedure to scale slope,
108 which is an important parameter in the topographical factors S and L of the RUSLE model. In
109 this scaling procedure slope was scaled from the GTOPO30 1km resolution digital elevation
110 model (USGS, 1996) to the coarser resolution of the erosion model based on high resolution OS
111 Ordnance (10m resolution) and SRTM data on elevation (90m resolution, International Centre
112 for Tropical Agriculture (CIAT), 2004) for England and Wales.

113 Doetterl et al. (2012) showed that together with the S factor, the rainfall erosivity or R factor
114 explain up to 75 % of the erosion variability across agricultural areas at the large watershed
115 scale, as these factors represent the triggers for soil erosion by providing energy for soil to erode.
116 The S and R factors can also be seen as the natural components of the RUSLE model, as they

117 have very little or no modification by human activities (Angulo-Martínez et al., 2009) apart from
118 indirect effects on precipitation and extreme events due to anthropogenic climate change that are
119 included in the *R* factor. In this way they represent the natural environmental constraints to soil
120 erosion that are important to capture before the effect of human activities on soil erosion through
121 land use change can be investigated. Previous studies on global soil erosion estimated the global
122 *R* factor based on the total annual precipitation (Renard and Freimund, 1994), due to the lack of
123 high resolution precipitation intensity on a global scale. However, high resolution precipitation
124 intensity is an important explaining parameter of the *R* factor and therefore, the applicability of
125 this method is limited.

126 The overall objective of this study is to extend the applicability of the RUSLE model to a coarse
127 resolution at a global scale, in order to enable future studies on the effects of soil erosion for the
128 past, current and future climate. To this end, we develop generally applicable methods that
129 improve the estimation of slope and climatic factors from coarse resolution global datasets.
130 These methods should not only be applicable across agricultural areas as in the studies of Van
131 Oost et al. (2007) and Doetterl et al. (2012), but also across non-agricultural areas. We adjust the
132 *S* factor to the coarse resolution of the global scale based on the scaling of slope according to the
133 fractal method. The adjustment of the *R* factor to the global scale is based on globally applicable
134 regression equations for different climate zones that include parameters for precipitation,
135 elevation and the simple precipitation intensity. This approach is validated using several high
136 resolution datasets on the *R* factor. Finally, the effects of these adjustments of both factors on
137 global soil erosion rates are investigated separately and tested against independent estimates of
138 soil erosion from high resolution and high precision datasets of Europe and the USA.

139

140 **2. Adjustment of the topographical factor**

141 **2.1 Scaling slope according to the fractal method**

142 The topographical factors of RUSLE are the slope steepness factor (*S*) and a slope length factor
143 (*L*). The *S* factor is generally computed by the continuous function of Nearing (1997):

$$144 \quad S = 1.5 + \frac{17}{1 + e^{(2.3 - 6.1 * \sin \theta)}} \quad (1)$$

145 And the *L* factor is computed according to Renard et al. (1997):

146 $L = \left(\frac{l}{22.13}\right)^m$ (2)

147 where: $m = \frac{F}{1+F}$ and $F = \frac{(\sin \theta / 0.0896)}{(3 * (\sin \theta)^{0.8} + 0.56)}$ (3)

148 in which θ is the slope and l is the slope length in meters.

149 As seen in the equations of the L and S factors, slope is a crucial parameter and thus an accurate
 150 estimation is essential in deriving accurate estimates of the L and S factors and finally also the
 151 soil erosion rates. For an accurate estimation of slope the input elevation data from digital
 152 elevation models (DEMs) should capture the detailed spatial variability in elevation. However,
 153 global DEMs are often too coarse to capture the detailed topography because of the surface
 154 smoothing effect. To account for this problem it is assumed that topography is fractal.
 155 Following Klinkenberg and Goodchild (1992) and Zhang et al. (1999), slope can be expressed as
 156 a function of the spatial scale by applying the variogram equation. The variogram equation is
 157 used to approximate the fractal dimension of topography and is expressed as follows:

158 $(Z_p - Z_q)^2 = k d_{pq}^{A-2D}$ (4)

159 so that:

160 $\frac{|Z_p - Z_q|}{d_{pq}} = \alpha d_{pq}^{1-D}$ (5)

161 where Z_p and Z_q are the elevations at points p and q , d_{pq} is the distance between p and q , k is a
 162 constant, $\alpha = k^{0.5}$ and D is the fractal dimension. Because the left side of Eq. (5) represents the
 163 slope, it can be assumed that the slope θ is related to the spatial scale or the grid size d in:

164 $\theta = \alpha d^{1-D}$ (6)

165 This result implies that by calculating the fractal properties (D and α) Eq. (6) can be used to
 166 calculate slope at any specified scale d . The local fractal dimension describes the roughness of
 167 the topography while the local value of α is related to the concept of lacunarity, which is a
 168 measure of the size of “gaps” (valleys and plains) in the topography (Zhang et al., 2002). To
 169 estimate the spatial variations of the fractal dimension D and the fractal coefficient α , Zhang et
 170 al. (1999) proposed to relate these parameters to the standard deviation of elevation. Hereby it is
 171 assumed that the standard deviation of elevation does not change much with the DEM resolution.

172 D is then calculated as a function of the standard deviation (σ) in a 3 x 3 pixels moving window
173 as proposed by Zhang et al. (1999):

$$174 \quad D = 1.13589 + 0.08452 \ln \sigma \quad (7)$$

175 To estimate α we used the modified approach by Pradhan et al. (2006), who derived α directly
176 from the steepest slope in a 3 x 3 pixels moving window, called $\alpha_{steepest}$ in the following. Having
177 obtained $\alpha_{steepest}$ and D from a grid at a given resolution, the scaled slope (θ_{scaled}) for a target grid
178 resolution d_{scaled} is obtained by:

$$179 \quad \theta_{scaled} = \alpha_{steepest} d_{scaled}^{1-D} \quad (8)$$

180 Pradhan et al. (2006) also showed that in their case study the ideal target resolution for
181 downscaling slope was 150m due the breakdown of the unifractal concept at very fine scales,
182 which they showed to happen at a scale of 50m. Altogether, this fractal method shows that a high
183 resolution slope can be obtained from a low resolution DEM as needed by the RUSLE model.

184

185 **2.2 Application of the fractal method on global scale**

186 In this study, we investigate the performance of the fractal method on a global scale using
187 different global DEMs as a starting point. The target resolution of downscaling is put to 150m
188 (about 5 arc-second) according to Pradhan et al. (2006). It should be noted that the original
189 spatial scale that the RUSLE and USLE models are operating on is usually between 10 and
190 100m, which indicates that the 150m target resolution may be still too coarse for a correct
191 representation of slope. The DEMs that are used here are given in Table 1.

192 As reported in previous studies (Zhang et al., 1999; Chang and Tsai, 1991; Zhang and
193 Montgomery, 1994), the average slope decreases with decreasing DEM resolution. This confirms
194 the expectation of loss of detail in topography at lower DEM resolutions. A large difference is
195 found between the unscaled global average slope of the 5 arc-minute and the 30 arc-second
196 DEMs, which is in the order of 0.017 m m^{-1} or 74 % (Table 2). After applying the fractal
197 method, the scaled slopes of the DEMs at 150 m target resolution are all increased significantly
198 compared to the unscaled slopes (Fig. 1). However, there is still a difference of about 0.05 m m^{-1}
199 or 8.5 % between the scaled slopes of the 5 arc-minute and the 30 arc-second DEMs (Table 2).

200 This difference can be attributed to several factors. One factor could be the underlying
201 assumption that the standard deviation of elevation (σ) is independent of the DEM resolution.
202 Although σ does not change much when considering different resolutions, there is still a general
203 decrease in mean global σ when going from the 5 arc-minute to the 30 arc-second DEM (Table
204 2). Due to the dependence of the fractal dimension D on σ (Zhang et al., 1999), a decrease of σ
205 leads to a decrease in D and therefore an increase in the scaled slope. Other factors that could
206 play a role here are the dependence of $\alpha_{steepest}$ on the steepest slope and the breakdown of the
207 fractal method at certain scales and in certain environments. Zhang et al. (1999) mentioned that
208 the scaling properties of slope are affected in very coarse resolution DEMs if σ changes
209 considerably. On the other hand, Pradhan et al. (2006) mentioned the breakdown of the fractal
210 method at very fine scales. This can indicate that the 150m target resolution is not appropriate for
211 some topographically complex regions in the world when downscaling from the DEMs used in
212 this study. Or based on the limitation of the fractal method as addressed by Zhang et al. (1999)
213 the DEMs used in this study are too coarse to scale down the slope to 150m accurately.

214 After applying the fractal method on a 30 arc-second resolution DEM, the scaled slope shows a
215 clear increase in detail, while the unscaled slope shows a strong smoothing effect (Fig. 2A and
216 2B). It is found that after scaling the slope values range from 0 to 85 degrees and are less than 2
217 degrees in 80% of the area. In contrast, all slope values are less than 45 degrees and range
218 between 0 and 2 degrees in 89% of this area when slope is computed directly from the 30 arc-
219 second DEM.

220 The scaled slope from the 30 arc-second DEM will be used in this study to estimate the global
221 soil erosion rates by the RUSLE model.

222

223 **3. Adjustment of the rainfall erosivity factor**

224 **3.1 The approach by Renard and Freimund (1994)**

225 Rainfall erosivity (R factor) is described by Hudson (1971) and Wischmeier and Smith (1978) as
226 the result of the transfer of the kinetic energy of raindrops to the soil surface. This causes a
227 detachment of soil and the downslope transport of the soil particles depending on the amount of
228 energy, rainfall intensity, soil type and cover, topography and management (Da Silva, 2004). The

229 original method of calculating erosivity is described by Wischmeier and Smith (1978) and
 230 Renard et al. (1997) as:

$$231 \quad R = \frac{1}{n} * \sum_{j=1}^n \sum_{k=1}^{m_j} (EI_{30})_k \quad (9)$$

232 where n is the number of years of records, m_j is the number of storms of a given year j , and EI_{30}
 233 is the rainfall erosivity index of a storm k . The event's rainfall erosivity index EI_{30} (MJ mm ha⁻¹
 234 h⁻¹) is defined as:

$$235 \quad EI_{30} = I_{30} * \sum_{r=1}^m e_r v_r \quad (10)$$

236 where e_r and v_r are, respectively, the unit rainfall energy (MJ ha⁻¹ mm⁻¹) and the rainfall depth
 237 (mm) during a time period r , and I_{30} is the maximum rainfall intensity during a time period of 30
 238 minutes (mm h⁻¹). The unit rainfall energy, e_r , is calculated for each time period as:

$$239 \quad e_r = 0.29 * (1 - 0.72 * e^{-0.05 * i_r}) \quad (11)$$

240 where i_r is the rainfall intensity during the time period (mm h⁻¹).

241 The information needed to calculate the R factor according to the method of Wischmeier and
 242 Smith (1978) is difficult to obtain on a large spatial scale or in remote areas. Therefore, different
 243 studies have been done on deriving regression equations for the R factor (Angulo-Martinez et al.,
 244 2009, Meusburger et al., 2012, Goovaerts, 1999, Diodato and Bellocchi, 2010). Most of these
 245 studies, however, concentrate on a specific area and can therefore not be implemented on the
 246 global scale. Studies on global soil erosion estimation by the RUSLE model or a modified
 247 version of it (Doetterl et al., 2012, van Oost et al., 2007, Montgomery et al., 2007, Yang et al.,
 248 2003) have all used the method of Renard and Freimund (1994). Renard and Freimund related
 249 the R factor to the total annual precipitation based on erosivity data available for 155 stations in
 250 the USA, shown in the following equation:

$$251 \quad R = 0.0483 * P^{1.61}, \quad P \leq 850 \text{ mm}$$

$$252 \quad R = 587.8 - 1.219 * P + 0.004105 * P^2, \quad P > 850 \text{ mm} \quad (12)$$

253 To test how this method performs globally, first the R factor was calculated in this study
 254 according to the method of Renard and Freimund (Eq. 12) using the 0.25 degree resolution
 255 annual precipitation data from the GPCC product (Table 1). Then, three regions were selected to

256 validate the resulting R values and their variability: the USA (EPA, 2001), Switzerland
257 (Meusburger et al., 2011), and the Ebro basin in Spain (Angulo-Martinez et al., 2009). For these
258 regions high resolution erosivity data are available obtained from pluviographic data from local
259 meteorological stations across the whole region.

260 Figure 3 shows that the R values computed with the Renard and Freimund method strongly
261 overestimate R when compared to the high resolution R data of the selected regions. For the USA
262 the R factor of Renard and Freimund shows an overall overestimation for western USA and for a
263 large part of eastern USA when compared to the high resolution R (Table 7 and Fig. 3A).
264 Especially a strong overestimation is seen for the north-west coast of the USA. This region is
265 known to have complex rainfall patterns due to the presence of mountains and high local
266 precipitation intensities with frequent snow fall (Cooper, 2011). It should be noted that the USA
267 is not a completely suited case study for testing the R values computed with the Renard and
268 Freimund method, as this method is based on data from stations in the USA. The available high
269 resolution data on the R factor from Switzerland and the Ebro basin are better suited for an
270 independent validation.

271 For Switzerland, which has a complex precipitation variability influenced by the relief of the
272 Alps (Meusburger et al., 2012), the R factor of Renard and Freimund shows a strong overall
273 overestimation when compared to the observed or high resolution R values (Table 7 and Fig.
274 3B). For the Ebro basin located in Spain, the observed R data were available for the period 1997-
275 2006 from Angulo-Martinez et al., 2009. Also here the method of Renard and Freimund
276 overestimates the R factor and is not able to model the high spatial variability of the R data
277 (Table 7 and Fig. 3C).

278

279 **3.2 The linear multiple regression approach using environmental factors**

280 To better represent the R factor on a global scale, the R estimation was based on the updated
281 Köppen-Geiger climate classification (Table 3 and Fig.4). The Köppen-Geiger climate
282 classification is a globally climate classification and is based on the vegetation distribution
283 connected to annual cycles of precipitation and temperature (Lohmann et al., 1993). The reason
284 for this approach is that this classification system includes annual cycles of precipitation and is
285 thus indirectly related to precipitation intensity. Based on this it is possible to derive regression

286 equations for the R factor that are applicable for each individual climate zone. This provides a
287 basis to calculate R with coarse resolution data on a globally scale.

288 As a basis for deriving the regression equations for the R factor for most climate zones the high
289 resolution R maps of the USA from EPA (2001) were used. The USA covers most of the world's
290 climate zones and is also the largest region with available high resolution R data. Linear multiple
291 regression was used to adjust R :

$$292 \log(R_i) = \beta_0 + \sum_{j=1}^n \beta_{ij} * \log(X_{ij}) + \varepsilon_i, \text{ for } i = 1, 2, \dots, n \quad (13)$$

293 where X is the independent explanatory variable, j is the number of explanatory variables, β is a
294 constant and ε is the residual.

295 The regression operates on one or more of the following parameters (X_j): total annual
296 precipitation (GPCC 0.25 degree product), mean elevation (ETOPO 5 DEM), and the simple
297 precipitation intensity index, SDII. It should be mentioned that the SDII was only available on a
298 very coarse resolution of 2.5 degree resolution for certain regions on earth, such as parts of
299 Europe and the USA. The SDII is calculated as the daily precipitation amount on wet days (≥ 1
300 mm) in a certain time period divided by the number of wet days in that period. Previous studies
301 that performed regression of R showed that precipitation and elevation were in most cases the
302 only explanatory variables. Here, the SDII is added as it is a simple representation of
303 precipitation intensity, which is an important explaining variable of R . The precipitation and
304 SDII datasets were rescaled to a 5 arc-minute resolution (corresponding to 0.0833 degree
305 resolution) to match the Köppen-Geiger climate classification data that was available at the
306 resolution of 6 arc-minute (corresponding to 0.1 degree). Furthermore, high resolution erosivity
307 data from Switzerland (Meusburger et al., 2011) and annual precipitation from the GPCC 0.5
308 degree product were used to derive the regression equations for R for the polar (E) climates,
309 which are not present in the USA. For the rest of the climate zones not present in the USA it was
310 difficult to obtain high resolution erosivity data. Therefore, for those climate zones the method of
311 Renard and Freimund was maintained to calculate erosivity. Also, if no clear improvement of the
312 R factor is found when using the new regression equations for a specific climate zone, the R
313 factor of Renard and Freimund is kept. Here, we mainly used the r^2 combined with the residual
314 standard error to evaluate if the new regression equations showed a clear improvement in the R
315 factor. From the climate zones where high resolution erosivity data was available, the Renard

316 and Freimund R factors were kept for the BWh and Csa climate zones. These are just two
317 climate zones out of the 17 evaluated ones, which shows that the regression method performs
318 better than the old method in most cases. All datasets for deriving the R factor are described in
319 Table 1.

320

321 **3.3 Application of the linear multiple regression method on a global scale**

322 Tables 4 and 5 show the resulting regression equations for climate zones for which initially a low
323 correlation was found between the R values calculated by the method of Renard and Freimund
324 and the high resolution or observed R values from the maps of EPA (2001) and Meusburger et al.
325 (2011). Figure 5 shows for each addressed climate zone how the method of Renard and
326 Freimund and the new regression equations compare to the observed R of the USA. For the Ds
327 climate zones the new regression equations showed only a slight improvement as compared to
328 the method of Renard and Freimund. Also for the E climate zones the new regression equations
329 still showed a significant bias. However, they performed much better compared to the method of
330 Renard and Freimund. For most of the addressed climate zones the simple precipitation intensity
331 index (SDII) explained a large part of the variability in the R factor. The elevation played a
332 smaller role here. Elevation can be an important explaining variable in regions with a high
333 elevation variability, which then affects the precipitation intensity. Furthermore, from Table 4
334 and Table 6 it can be concluded that the R factor in f climate zones, which have no dry season,
335 can be easily explained by the total annual precipitation and the SDII. Dry climate zones,
336 especially dry summer climate zones showed a weaker correlation, which is most probably due
337 to the fact that the SDII is too coarse to explain the variability in the low precipitation intensity in
338 the summer. It is also interesting to see that even though the SDII was derived from a very coarse
339 dataset, it turned out to be still important for deriving more accurate R values. Furthermore,
340 Table 6 showed for each addressed climate zone a comparison of the newly computed average R
341 factor with the average observed R factor, and the uncertainty range. The uncertainty range was
342 computed by taking into account the standard deviation of each of the parameters in the
343 regression equations. As mentioned before, the E climate zones showed the largest uncertainty
344 range. The new regression equations significantly improved the R values and spatial variability
345 in the western USA and lead to a mean R factor that was closer to the data mean (Table 7 and

346 Fig. 6A). Although the new regression equations showed a bias for the E climate zones (the
347 minimum and maximum R were not captured), the resulting mean R for Switzerland showed a
348 strong improvement (Table 7 and Fig. 6B). Furthermore, the variability in the estimated R
349 compared well with the variability of the observed R . It should be noted that Switzerland is not
350 an independent case study anymore for the E climate zones. However, the Ebro basin case study
351 confirms that the improvement for the E climate zones that also occur here, is significant (Fig.
352 6C). As the observed R values of the USA and Switzerland were used to derive the regression
353 equations, the third case study, the Ebro basin in Spain, provided an important independent
354 validation. For the Ebro basin, the new regression equations not only improved the overall mean
355 but also captured the minimum R values better, resulting in an improved representation of the R
356 variability (Table 7 and Fig. 6C). In Fig. 6C, however, there was a clear pattern separation in the
357 newly computed R values, which was due to the fact that the SDII data were not available for
358 part of the Ebro basin. As mentioned before, SDII is an important explaining parameter in the
359 regression equations for most of the addressed climate zones.

360 Figure 7A showed the global patterns of the estimated R from respectively the method of Renard
361 and Freimund and the new regression equations. Figure 7B showed a difference plot between the
362 estimated R with the method of Renard and Freimund and the R estimated with the new
363 regression equations. The new regression equations significantly reduced the R values in most
364 regions. However, the tropical regions still showed unrealistic high R values (maximum R values
365 go up to $1 * 10^5$ MJ mm ha⁻¹ h⁻¹ yr⁻¹). This is because the R factor was not adjusted for the
366 tropical climate zones due to the lack of high resolution R data. Oliveira et al. (2012) found for
367 the R factor in Brazil that the maximum R values for the tropical climate zones reach 22,452 MJ
368 mm ha⁻¹ h⁻¹ yr⁻¹.

369 Finally, it should be noted that the purpose of the adjusting methods in this study is to capture
370 more accurately the large scale mean erosion rates rather than the extremes. Therefore, even
371 though the new regression equations are still not accurate enough for certain climate zones, it is
372 important that the mean R factor is represented well. The approach for adjusting the R factor also
373 showed that even though there is no high temporal resolution precipitation intensity data
374 available on a global scale, the R factor can still be represented well for most climate zones on a
375 large spatial scale by using other parameters, such as elevation, and especially a representative of
376 precipitation intensity, such as the SDII. The SDII played an important role here as it improved

377 the estimation of the *R* factor significantly, even though data was only available at a very low
378 resolution as compared to the other datasets of precipitation, elevation and climate zone
379 classification.

380

381 **4 Global application of the adjusted RUSLE model**

382 **4.1 Computation of the soil erodibility and crop cover factors**

383 In the following the consequences of the new parameterizations of the *S* and *R* factors for global
384 soil erosion rates are demonstrated. First, the other individual RUSLE factors, soil erodibility (*K*)
385 and crop cover (*C*) needed to be computed. Estimations of the *K* factor were based on soil data
386 from the gridded 30 arc-second Global Soil Dataset for use in Earth System Models (GSCE).
387 GSCE is based on the Harmonized World Soil database (HWSD) and various other regional and
388 national soil databases (Shangguan et al., 2014). The method of Torri et al. (1997) was then used
389 to estimate the *K* factor. Volcanic soils were given a *K* factor of $0.08 \text{ t ha h ha}^{-1} \text{ MJ}^{-1} \text{ mm}^{-1}$, as
390 these soil types are usually very vulnerable for soil erosion and the *K* values are beyond the
391 range predicted by the method of Torri et al. (1997) (van der Knijff et al., 1999). To account for
392 the effect of stoniness on soil erosion a combination of the methods used by Cerdan et al. (2010)
393 and Doetterl et al. (2012) was applied, who base their methods on the original method of Poesen
394 et al. (1994). For non-agricultural areas the method of Cerdan et al. (2010) was used where they
395 reduced the total erosion by 30 % for areas with a gravel percentage larger or equal to 30%. For
396 agricultural and grassland areas the method of Doetterl et al. (2012) was used, where erosion was
397 reduced by 80 % in areas where the gravel percentage exceeded 12%.

398 The *C* factor was calculated according to the method of De Jong et al. (1998), using 0.25 degree
399 Normalized Difference Vegetation Index (NDVI) and land use data for the year 2002. An
400 important limitation of this method is the fact that in winter the *C* factor is estimated too large
401 (van der Knijff et al., 1999). This is because the equation does not include the effects of mulch,
402 decaying biomass and other surface cover reducing soil erosion. To prevent the *C* factor of being
403 too large, maximum *C* values for forest and grassland of 0.01 and 0.05 for pasture were used.
404 Doetterl et al. (2012) showed that the slope length (*L*) and support practice (*P*) factors do not
405 contribute significantly to the variation in soil erosion at the continental scale to global scale,
406 when compared to the contribution of the other RUSLE factors (*S*,*R* and *C*). However, this does

407 not mean that their influence on erosion should be ignored completely. They may play an
408 important role in local variation of erosion rates. In our erosion calculations we do not include
409 these factors, because we have too little to no data on these factors on a global scale. Including
410 them in the calculations would only add an additional large uncertainty to the erosion rates,
411 which would make it more difficult to judge the improvements we made to the *S* and *R* factors.

412

413 **4.2 Computation of global soil erosion and comparison to empirical databases**

414 The RUSLE model with the settings mentioned in the previous paragraph is applied on a 5 arc-
415 minute resolution on a global scale for the present time period (see time resolutions of datasets in
416 Table 1). Global soil erosion rates are calculated for four different versions of the RUSLE model:
417 (a) the unadjusted RUSLE, (b) RUSLE with only an adjusted *S* factor, (c) RUSLE with only an
418 adjusted *R* factor and (d) the adjusted RUSLE (all adjustments included). The global mean soil
419 erosion rate for the adjusted RUSLE is found to be $7 \text{ t ha}^{-1} \text{ y}^{-1}$ (Fig. 8A). When including the
420 uncertainty arising from applying the linear multiple regression method, the mean global soil
421 erosion rate differs between 6 and $18 \text{ t ha}^{-1} \text{ y}^{-1}$. Furthermore, the RUSLE version with only an
422 adjusted *S* factor shows the highest mean global soil erosion rate, while the lowest rate is found
423 for the RUSLE version with only the adjusted *R* factor (Table 8). From the global map showing
424 the difference between the erosion rates of the *S* adjusted RUSLE and the unadjusted RUSLE
425 versions (Fig. 8C) one can see that erosion rates are in general increased and mostly pronounced
426 in mountainous regions. This feature is ‘dampened’ by adjusting the *R* factor. Looking at the
427 global map showing the difference between the *R* adjusted RUSLE and unadjusted RUSLE
428 versions (Fig. 8D), one can see that the erosion rates are overall decreased in regions where the
429 adjustments are made. When combining both adjustments of the RUSLE model in the fully
430 adjusted RUSLE version and subtract the unadjusted RUSLE erosion rates (Fig. 8B), one can see
431 that the erosion rates are slightly decreased in areas where the *R* factor is adjusted. However, in
432 the tropics for example there is an increase in erosion rates by the fully adjusted RUSLE due to
433 the lack of adjusting the *R* factor there. This indicates that these two factors balance each other,
434 and that it is important to have a correct representation of all the RUSLE factors on a global scale
435 in order to predict reliable erosion rates.

436 In this study the K and C factors are not tested and adjusted for a coarse resolution at the global
437 scale and thus validation with existing empirical databases on soil erosion is not fully justified.
438 However, to test if the global erosion rates are in an acceptable range, they are compared to
439 erosion estimates from the NRI database for the USA and erosion estimates from the study of
440 Cerdan et al. (2010) for Europe. These are to our knowledge the only large scale high resolution
441 empirical databases on soil erosion.

442 The NRI database contains USLE erosion estimates for the year 1997, which are available at the
443 HUC4 watershed level. After aggregating the resulting erosion rates from the adjusted and
444 unadjusted RUSLE models to the HUC4 watershed level, the results showed that the mean
445 erosion rates from the adjusted RUSLE model come closer to that of the NRI database (Table 9
446 and Fig. 9A). However, the maximum observed mean HUC4 soil erosion rate from the adjusted
447 RUSLE was twice as high as compared to the NRI database. This maximum is observed in the
448 hilly and relatively wet region on the west coast of the USA. From these results we can conclude
449 that the erosion rates of the adjusted RUSLE fall in the range of observed values, but that there
450 are still some local overestimations. For example, the north west of the US shows a slightly
451 worse performance in the adjusted model most probably because in this region the estimation of
452 the R factor could not be improved, while the S factor is increased. This gives an overall increase
453 in soil erosion rates. In this region of the USA, the Csb climate prevails, for which the R factor is
454 still difficult to estimate in a correct way (Table 4). So for this climate there are some outliers in
455 the R factor in this specific region.

456 For Europe, Cerdan et al. (2010) used an extensive database of measured erosion rates on plots
457 under natural rainfall. They extrapolated measured erosion rates to the whole Europe (European
458 Union area) and adjusted them with a topographic correction based on the L and S factors of
459 RUSLE, and a correction to account for soil stoniness. For comparison, the soil erosion rates
460 from Cerdan et al. (2010) and the RUSLE estimates are aggregated at country level. The
461 performance of the adjusted RUSLE model was not as good for Europe compared to the USA,
462 which is not surprising due to the fact that the RUSLE model is based on soil erosion data of the
463 USA. However, also on the European scale the adjusted RUSLE model performed better than the
464 unadjusted RUSLE model (Table 9 and Fig. 9B). Especially the large erosion rates in the south
465 of Europe as observed in the results of the unadjusted RUSLE model are less extreme for the

466 adjusted RUSLE model results. Still, the overall mean erosion rate for Europe was overestimated
467 by approximately two times (Table 9).

468 These biases in erosion rates as seen for the USA and Europe can be attributed to several factors.
469 Firstly, the other RUSLE factors (K and C) and the way they interact with each other are not
470 adjusted to the coarse resolution of the global scale. From figures 8, which provide global
471 erosion rates, no clear signal can be found for which land cover types the RUSLE performs
472 worse or better. In general, we can see that the adjusted RUSLE model still overestimates
473 erosion rates for most land cover types. A short analysis for Europe showed that the largest
474 biases are found for shrubs, and the least for grassland. However, a more explicit analysis is
475 needed here to find out how we can improve the contribution of land cover and land use to
476 erosion rates in the RUSLE model. For example looking at the location of land use in a certain
477 grid cell could make a difference in the resulting erosion rates. If the land use in a grid cell is
478 located on steep slopes the resulting erosion in that gridcell would be higher than when it would
479 be located in the flatter areas. In this study, however, only mean fractions of land cover and the
480 NDVI are used for each gridcell, which can lead to possible biases in the resulting erosion rates.
481 Secondly, land management is not accounted for in this study, which could introduce an
482 important systematic bias in the soil erosion rates for especially agricultural areas. Furthermore,
483 uncertainties in the coarse resolution land cover/land use, soil and precipitation datasets that are
484 not accounted for, can lead to the model biases. Also, better adjustment of the R factor for
485 climate zones such as the E climate zones, could help improving the overall results. Some biases
486 in the erosion rates can also be attributed to the fact that stepped relief, where flat plateaus are
487 separated by steep slopes, are not well captured by the 150m target resolution used in the fractal
488 method to scale slope. In this way erosion would be overestimated in these areas. Finally, errors
489 and limitations in the observational datasets can also contribute to the differences between model
490 and observations. The study of Cerdan et al. (2010) on Europe for example used extrapolation of
491 local erosion data to larger areas that could introduce some biases. Also the underlying studies on
492 measured erosion rates used different erosion measuring techniques that can be linked to
493 different observational errors.

494

495 **5 Conclusions**

496 In this study we introduced specific methods to adjust the topographical and rainfall erosivity
497 factors to improve the application of the RUSLE model on a global scale using coarse resolution
498 input data.

499 Our results show that the fractal method by Zhang et al. (1999) and Pradhan et al. (2006) can be
500 applied on coarse resolution DEMs to improve the resulting slope. Although the slope
501 representation improved after applying this method, the results still show a slight dependence on
502 the original grid resolution. This is attributable to several factors such as the underlying
503 assumption that the standard deviation of elevation (σ) is independent of the DEM resolution,
504 and to the breakdown of the fractal method at certain scales.

505 We compared the rainfall erosivity calculated by the method of Renard and Freimund to
506 available high resolution or observed erosivity data of the USA, Switzerland and the Ebro basin,
507 and showed overall significant biases. We implemented a linear multiple regression method to
508 adjust erosivity for climate zones of the Köppen-Geiger climate classification system in the USA
509 that showed a bias in erosivity calculated with the method of Renard and Freimund. Using
510 precipitation, elevation and the simple precipitation intensity index as explaining parameters, the
511 resulting adjusted erosivity compares much better to the observed erosivity data for the USA,
512 Switzerland and the Ebro basin. Not only the mean values but also the spatial variability in
513 erosivity is improved. It was surprising to notice that using the rather coarse resolution simple
514 precipitation intensity index in the regression analysis made it possible to explain much of the
515 variability in erosivity. This, once more, underpins the importance of precipitation intensity in
516 erosivity estimation.

517 After calculating the newly adjusted erosivity on a global scale, it is apparent that the tropical
518 climate zones, for which erosivity was not adjusted, show strong overestimations in some areas
519 when compared to estimated erosivity from previous studies. This shows that adjusting erosivity
520 for the tropical climate zones should be the next step. The challenge is to find enough reliable
521 long term and high resolution erosivity data for those regions.

522 To investigate how the adjusted topographical and rainfall erosivity factors affect the global soil
523 erosion rates, we applied the adjusted RUSLE model on a global scale and estimate a mean
524 global soil erosion rate of $7 \text{ t ha}^{-1} \text{ y}^{-1}$. It is, however, difficult to provide accurate uncertainty
525 estimates to the global erosion rates of this study and to provide a good validation with

526 observations, due to lack of high resolution data on other individual RUSLE factors such as the
527 soil erodibility, slope length and support practice. These RUSLE factors, together with the crop
528 cover factor, which includes the effects of land use, are therefore not adjusted for application on
529 a coarse resolution on global scale.

530 To test if the soil erosion rates from the adjusted RUSLE model are in a realistic range, we
531 compared the results to the USLE erosion estimates for the USA from the NRI database and the
532 erosion estimates for Europe from the study of Cerdan et al. (2010). The adjusted RUSLE soil
533 erosion rates, which we aggregated to the HUC4 watershed level, show a better comparison with
534 the NRI USLE estimates for the USA than the unadjusted RUSLE erosion rates. For Europe the
535 comparison of the adjusted RUSLE soil erosion rates to the study of Cerdan et al. (2010) were
536 not as good as for the USA. This is not surprising due to the fact that the parameterizations of the
537 RUSLE model are based on soil erosion data of the USA. However, also for Europe, the adjusted
538 RUSLE model performs better than the unadjusted RUSLE model.

539 We find strong overestimations by the adjusted RUSLE model for hilly regions in the west coast
540 of the USA and for south of Europe. We argue that besides for reasons mentioned before, these
541 biases are due to the fact that the topographical detail may not be enough in some regions to
542 capture the true variability in soil erosion effects by topography. Also erosivity could not be
543 adjusted for some climate zones that are not present in the USA or Switzerland, and needs to be
544 improved for climate zones such as the polar climate zones.

545 We conclude that even though there is still much improvement of the RUSLE model possible
546 with respect to topography and erosivity, the methods proposed in this study seem to be
547 promising tools for improving the global applicability of the RUSLE model. A globally
548 applicable version of the RUSLE model together with data on environmental factors from Earth
549 System Models (ESMs) can provide the possibility for future studies to estimate accurate soil
550 erosion rates for the past, current and future time periods.

551

552 **Acknowledgements**

553

554 We like to thank the anonymous reviewers for their useful comments. The article processing
555 charges for this open-access publication have been covered by the Max Planck Society.

556 **References**

- 557 1 Amante, C. and Eakins, B. W.: ETOPO1 1 Arc-Minute Global Relief Model: Procedures,
558 Data Sources and Analysis, NOAA Technical Memorandum NESDIS NGDC-24,
559 National Geophysical Data Center, NOAA, 2009.
- 560 2 Angulo-Martínez, M., López-Vicente, M., Vicente-Serrano, S. M. and Beguería, S.:
561 Mapping rainfall erosivity at a regional scale: a comparison of interpolation methods in
562 the Ebro Basin (NE Spain), *J. Hydrol. Earth Syst. Sc.*, 13, 1907-1920, 2009,
563 <http://www.hydrol-earth-syst-sci.net/13/1907/2009/>.
- 564 3 Bork, H. R. and Lang A.: Quantification of past soil erosion and land use / land cover
565 changes in Germany, in: Long term hillslope and fluvial system modelling. Concepts and
566 case studies from the Rhine river catchment, *Lecture Notes in Earth Sc.*, 101, 231-239,
567 2003.
- 568 4 Cerdan, O., Govers, G., Le Bissonnais, Y., Van Oost, K., Poesen, J., Saby, N., Gobin, a.,
569 Vacca, a., Quinton, J., Auerswald, K., Klik, a., Kwaad, F. J. P. M., Raclot, D., Ionita, I.,
570 Rejman, J., Rouseva, S., Muxart, T., Roxo, M. J. and Dostal, T.: Rates and spatial
571 variations of soil erosion in Europe: A study based on erosion plot data, *Geomorphology*,
572 122(1-2), 167–177, doi:10.1016/j.geomorph.2010.06.011, 2010.
- 573 5 Chang, K. T. and Tsai, B. W.: The effect of DEM resolution on slope and aspect
574 mapping, *Cartography and Geographic Information Systems*, 18(1), 69-77, 1991.
- 575 6 Cooper K.: Evaluation of the Relationship between the RUSLE R-Factor and Mean
576 Annual Precipitation, available at:
577 [http://www.engr.colostate.edu/~pierre/ce_old/Projects/linkfiles/Cooper%20R-factor-](http://www.engr.colostate.edu/~pierre/ce_old/Projects/linkfiles/Cooper%20R-factor-Final.pdf)
578 [Final.pdf](http://www.engr.colostate.edu/~pierre/ce_old/Projects/linkfiles/Cooper%20R-factor-Final.pdf) (last access: 15 January 2015), 2011.
- 579 7 Da Silva, A. M.: Rainfall erosivity map for Brazil, *Catena*, 57(3), 251–259,
580 doi:10.1016/j.catena.2012.08.006, 2004.
- 581 8 De Jong, S. M., Brouwer, L. C. and Riezebos, H. Th.: Erosion hazard assessment in the
582 Peyne catchment, France, Working paper DeMon-2 Project, Dept. Physical Geography,
583 Utrecht University, 1998.

- 584 9 Diodato, N. and Bellocchi, G.: MedREM, a rainfall erosivity model for the
585 Mediterranean region, *J. Hydrol.*, 387(1-2), 119–127, doi:10.1016/j.jhydrol.2010.04.003,
586 2010.
- 587 10 Doetterl, S., Van Oost, K. and Six, J.: Towards constraining the magnitude of global
588 agricultural sediment and soil organic carbon fluxes, *Earth Surf. Process. Landforms*,
589 37(6), 642–655, doi: 10.1002/esp.3198, 2012.
- 590 11 Donat, M. G., Alexander, L.V., Yang, H., Durre, I., Vose, R. and Caesar, J.: Global
591 Land-Based Datasets for Monitoring Climatic Extremes, *Bulletin American*
592 *Meteorological Society*, 94, 997–1006, 2013.
- 593 12 Friedl, M. A., Strahler, A. H. and Hodges, J.: ISLSCP II MODIS (Collection 4) IGBP
594 Land Cover, 2000-2001. In Hall, Forest G., G. Collatz, B. Meeson, S. Los, E. Brown de
595 Colstoun, and D. Landis (eds.), ISLSCP Initiative II Collection, edited by: Hall, F. G.,
596 Collatz, G., Meeson, B., Los, S., Brown de Colstoun, E., and Landis, D., from Oak Ridge
597 National Laboratory Distributed Active Archive Center, Oak Ridge, Tennessee, U.S.A.,
598 available online at: <http://daac.ornl.gov/> (last access: 15 January 2015), 2010.
- 599 13 Gesch, D.B., Verdin, K.L. and Greenlee, S.K.: New land surface digital elevation model
600 covers the earth, *Eos, Transactions, AGU*, 80(6), 69–70, doi: 10.1029/99EO00050, 1999.
- 601 14 Goll, D. S., Brovkin, V., Parida, B. R., Reick, C. H., Kattge, J., Reich, P. B., van
602 Bodegom, P. M. and Niinemets, Ü.: Nutrient limitation reduces land carbon uptake in
603 simulations with a model of combined carbon, nitrogen and phosphorus cycling,
604 *Biogeosciences*, 9, 3547–3569, doi:10.5194/bg-9-3547-2012, 2012.
- 605 15 Goovaerts, P.: Using elevation to aid the geostatistical mapping of rainfall erosivity,
606 *Catena*, 34, 227–242, doi:10.1016/S0341-8162(98)00116-7, 1999.
- 607 16 Gruber, N. and Galloway, J. N.: An Earth-system perspective of the global nitrogen
608 cycle., *Nature*, 451, 293–6, doi:10.1038/nature06592, 2008.
- 609 17 Hall, F. G., Brown de Colstoun, E., Collatz, G. J., Landis, D., Dirmeyer, P., Betts, A.,
610 Huffman, G. J., Bounoua, L. and Meeson, B.: ISLSCP Initiative II global data sets:
611 Surface boundary conditions and atmospheric forcings for land-atmosphere studies, *J.*
612 *Geophys. Res.*, 111, D22S01, doi:10.1029/2006JD007366, 2006.

- 613 18 Hooke, R. L.: On the history of humans as geomorphic agents, *Geology*, 28, 843–846,
614 doi:10.1130/0091-7613(2000)28<843:OTHOHA>2.0.CO;2, 2000.
- 615 19 Hudson N.: *Soil Conservation*, Cornell University Press, Ithaca, 1971.
- 616 20 Ito, A.: Simulated impacts of climate and land-cover change on soil erosion and
617 implication for the carbon cycle, 1901 to 2100, *Geophys. Res. Lett.*, 34, L09403,
618 doi:10.1029/2007GL029342, 2007.
- 619 21 Klinkenberg, B. and Goodchild, M. F.: The fractal properties of topography: A
620 comparison of methods, *Earth Surf. Process. Landforms*, 17, 217-234,
621 doi:10.1002/esp.3290170303, 1992.
- 622 22 Lal, R.: Soil erosion and the global carbon budget, *Environ. Int.*, 29, 437–50,
623 doi:10.1016/S0160-4120(02)00192-7, 2003.
- 624 23 Lohmann, U., Sausen, R., Bengtsson, L., Cubasch, U., Perlwitz, J. and Roeckner, E.: The
625 Köppen climate classification as a diagnostic tool for general circulation models, *Climate*
626 *Res.*, 3, 177-193, 1993.
- 627 24 Meusburger, K., Steel, a., Panagos, P., Montanarella, L. and Alewell, C.: Spatial and
628 temporal variability of rainfall erosivity factor for Switzerland, *Hydrol. Earth Syst. Sci.*
629 *Discuss.*, 8, 8291–8314, doi:10.5194/hessd-8-8291-2011, 2011.
- 630 25 Meusburger, K., Steel, a., Panagos, P., Montanarella, L. and Alewell, C.: Spatial and
631 temporal variability of rainfall erosivity factor for Switzerland, *Hydrol. Earth Syst. Sci.*,
632 16, 167–177, doi:10.5194/hess-16-167-2012, 2012.
- 633 26 Meyer-Christoffer, A., Becker, A., Finger, P., Rudolf, B., Schneider, U. and Ziese, M.:
634 GPCC Climatology Version 2011 at 0.25°: Monthly Land-Surface Precipitation
635 Climatology for Every Month and the Total Year from Rain-Gauges built on GTS-based
636 and Historic Data, 2011.
- 637 27 Milliman, J. D. and Syvitski, J. P. M.: Geomorphic / Tectonic Control of Sediment
638 Discharge to the Ocean : The Importance of Small Mountainous Rivers, *J. Geology*, 100,
639 525–544, 2014.

- 640 28 Montgomery, D. R.: Soil erosion and agricultural sustainability, *PNAS*, 104, 13268–
641 13272, doi: 10.1073/pnas.0611508104, 2007.
- 642 29 National Geophysical Data Center/NESDIS/NOAA/U.S. Department of Commerce:
643 TerrainBase, Global 5 Arc-minute Ocean Depth and Land Elevation from the US
644 National Geophysical Data Center (NGDC), Research Data Archive at the National
645 Center for Atmospheric Research, Computational and Information Systems Laboratory,
646 available online at: <http://rda.ucar.edu/datasets/ds759.2/> (last access 30 November 2014),
647 1995.
- 648 30 Nearing, M.A.: A single, continuous function for slope steepness influence on soil loss,
649 *Soil. Sci. Soc. Am. J.*, 61: 917-929, doi:10.2136/sssaj1997.03615995006100030029x,
650 1997.
- 651 31 Oliveira, P. T. S., Wendland, E. and Nearing, M. A.: Rainfall erosivity in Brazil: A
652 review, *Catena*, 100, 139–147, doi:10.1016/j.catena.2012.08.006, 2013.
- 653 32 Peel, M. C., Finlayson, B. L. and McMahon, T. A.: Updated world map of the Köppen-
654 Geiger climate classification, *HESS*, 1633–1644, 2007.
- 655 33 Pimentel, D., Harvey, C., Resosudarmo, P., Sinclair, K., Kurz, D., McNair, M., Cris, S.,
656 Shpritz, L., Fitton, L., Saffouri, R. and Blair, R.: Environmental and economic costs of
657 soil erosion and conservation benefits, *Science*, 267, 1117-1123, 1995.
- 658 34 Poesen, J., Nachtergaele, J., Verstraeten, G. and Valentin, C.: Gully erosion and
659 environmental change: importance and research needs, *Catena*, 50, 91–133,
660 doi:10.1016/S0341-8162(02)00143-1, 2003.
- 661 35 Pradhan, N. R., Tachikawa, Y. and Takara, K.: A downscaling method of topographic
662 index distribution for matching the scales of model application and parameter
663 identification, *Hydrol. Process.*, 20, 1385–1405, doi:10.1002/hyp.6098, 2006.
- 664 36 Quinton, J. N., Govers, G., Van Oost, K. and Bardgett, R. D.: The impact of agricultural
665 soil erosion on biogeochemical cycling, *Nat. Geosci.*, 3, 311–314, doi:10.1038/ngeo838,
666 2010.
- 667 37 Regnier, P., Friedlingstein, P., Ciais, P., Mackenzie, F. T., Gruber, N., Janssens, I. A.,
668 Laruelle, G. G., Lauerwald, R., Luysaert, S., Andersson, A. J., Arndt, S., Arnosti, C.,

669 Borges, A. V., Dale, A. W., Gallego-Sala, A., Godd eris, Y., Goossens, N., Hartmann, J.,
670 Heinze, C., Ilyina, T., Joos, F., LaRowe, D. E., Leifeld, J., Meysman, F. J. R., Munhoven,
671 G., Raymond, P. a., Spahni, R., Suntharalingam, P. and Thullner, M.: Anthropogenic
672 perturbation of the carbon fluxes from land to ocean, *Nat. Geosci.*, 6(8), 597–607,
673 doi:10.1038/ngeo1830, 2013.

674 38 Reich, P. B. and Hungate, B. A.: Carbon-Nitrogen in Terrestrial Interactions in Response
675 Ecosystems to Rising Atmospheric Carbon Dioxide, *Annu. Rev. Ecol. Evol. Syst.*, 37,
676 611–636, doi:10.2307/annurev.ecolsys.37.091305.30000023, 2006.

677 39 Renard, K. G. and Freimund, J. R.: Using monthly precipitation data to estimate the R-
678 Factor in the revised USLE, *J. Hydrol.*, 157, 287-306, doi:10.1016/0022-1694(94)90110-
679 4, 1994.

680 40 Renard, K. G., Foster, G. R., Weesies, G.A., Mccool, D. K. and Yoder, D. C.: Predicting
681 Soil Erosion by Water: a Guide to Conservation Planning with the Revised Universal Soil
682 Loss Equation (RUSLE), *Agriculture Handbook 703*, USDA, 1997.

683 41 Schneider, U., Becker, A., Finger, P., Meyer-Christoffer, A., Rudolf, B. and Ziese, M.:
684 GPCP Full Data Reanalysis Version 6.0 at 0.5 : Monthly Land-Surface Precipitation
685 from Rain-Gauges built on GTS-based and Historic Data, 2011.

686 42 Shangguan, W., Dai, Y., Duan, Q., Liu, B. and Yuan, H.: A Global Soil Data Set for
687 Earth System Modeling, *J. Adv. Model. Earth Syst.*, 6, 249-263, doi:
688 10.1002/2013MS000293, 2014.

689 43 Stallard, R. F.: Terrestrial sedimentation and the carbon cycle: Coupling weathering and
690 erosion to carbon burial, *Global Geochem. Cy.*, 12, 231–257, doi:10.1029/98GB00741,
691 1998.

692 44 Thornton, P. E., Lamarque, J.-F., Rosenbloom, N. a. and Mahowald, N. M.: Influence of
693 carbon-nitrogen cycle coupling on land model response to CO 2 fertilization and climate
694 variability, *Global Biogeochem. Cycles*, 21, n/a–n/a, doi:10.1029/2006GB002868, 2007.
695

- 696 45 Torri, D., Poesen, J. and Borselli, L.: Predictability and uncertainty of the soil erodibility
697 factor using a global dataset, *Catena*, 31, 1-22, doi:10.1016/S0341-8162(97)00036-2,
698 1997.
- 699 46 Tucker, C., Pinzon, J., Brown, M., Slayback, D., Pak, E., Mahoney, R., Vermote, E. and
700 El Saleous, N.: An extended AVHRR 8-km NDVI dataset compatible with MODIS and
701 SPOT vegetation NDVI data, *Int. J. Remote Sens.*, 26, 4485–4498, 2005.
- 702 47 United Nations Convention to Combat Desertification (UNCCD): Zero Net Land
703 Degradation, 2012.
- 704 48 United States Environmental Protection Agency: Stormwater Phase 2 Final Rule,
705 Construction Rainfall Erosivity Waiver, EPA 833-F-00-014, 2001.
- 706 49 US Department of Agriculture: Summary Report: 1997 National Resources Inventory
707 (revised December 2000), Natural Resources Conservation Service, Washington, DC,
708 and Statistical Laboratory, Iowa State University, Ames, Iowa, 2000.
- 709 50 US Department of Commerce, National Oceanic and Atmospheric Adminis.: 2-minute
710 Gridded Global Relief Data (ETOPO2), 2001.
- 711 51 US Geological Survey.: GTOPO30 Arc-Second Elevation Data Set, EROS Data Center
712 (EDC) Distributed Active Archive Center (DAAC), Sioux Falls, available online at:
713 <http://edcdaac.usgs.gov/gtopo30/gtopo30.html> (last access 15 January 2015), 1996.
- 714 52 Van der Knijff, J. M., Jones, R. J. A. and Montanarella, L.: Soil Erosion Risk Assessment
715 in Italy, Joint Research Center, EUR19022EN, European Commission, 1999.
- 716 53 Van Oost, K., Quine, T. a, Govers, G., De Gryze, S., Six, J., Harden, J. W., Ritchie, J. C.,
717 McCarty, G. W., Heckrath, G., Kosmas, C., Giraldez, J. V, da Silva, J. R. M. and
718 Merckx, R.: The impact of agricultural soil erosion on the global carbon cycle, *Science*,
719 318(5850), 626–9, doi:10.1126/science.1145724, 2007.
- 720 54 Wilkinson, B. H. and McElroy, B. J.: The impact of humans on continental erosion and
721 sedimentation, *Geol. Soc. Am. Bull.*, 119, 140–156, doi:10.1130/B25899.1, 2007.
- 722 55 Wischmeier, W. H. and Smith, D. D.: Predicting Rainfall Erosion Losses. A guide to
723 conservation planning, *Agricultural Handbook 537*, USDA, Washington, 58 pp, 1978.

- 724 56 Yang, D., Kanae, S., Oki, T., Koike, T. and Musiake, K.: Global potential soil erosion
725 with reference to land use and climate changes, *Hydrol. Process.*, 17, 2913–2928,
726 doi:10.1002/hyp.1441, 2003.
- 727 57 Zhang, W. and Montgomery, D. R.: Digital elevation model grid size, landscape
728 representation, and hydrologic simulations, *Water Resour. Res.*, 30, 1019-1028,
729 doi:10.1029/93WR03553, 1994.
- 730 58 Zhang, X., Drake, N. and Wainwright, J.: Scaling land surface parameters for global-
731 scale soil erosion estimation, *Water Resour. Res.*, 38, 19–1–19–9,
732 doi:10.1029/2001WR000356, 2002.
- 733

Table 1. List of datasets used in this study

Category	Dataset	Source	Spatial resolution	Temporal-period	Variables
DEM	GTOPO Elevation Model	USGS, 1996, Gesch et al., 1999	30 arc-seconds		elevation
	ETOPO1 Elevation Model	Amante and Eakins, 2009	1 arc-minute		elevation
	ETOPO2 Elevation Model	US Department of Commerce and NOAA, 2001	2 arc-minute		elevation
	ETOPO5 Elevation Model	National Geophysical Data Center/NESDIS/NOAA, 1995	5 arc-minute		elevation
Climate	GPCC 0.5 degree dataset	Schneider et al., 2011	0.5 degrees	Years 1989-2010	total yearly precipitation
	GPCC 0.25 degree	Meyer-Christoffer et al.,	0.25 degrees	years 1951-	total yearly

	dataset	2011		2000	precipitation
	GHCNDEX dataset	CLIMDEX (Donat et al., 2013)	2.5 degrees	years 1951-present	simple precipitation intensity index (SDII)
	Köppen-Geiger dataset	Peel et al., 2007	5 arc-minute		Köppen-Geiger climate classifications
Soil	Global Soil Dataset for use in Earth System Models (GSCE)	Shangguan et al., 2014	30 arc-seconds		sand, silt and clay fractions, organic matter %, gravel %
	Harmonized World Soil Database (HWSD) version 1.2	Nachtergaele et al., 2012	30 arc-seconds		volcanic soils
Land-cover	GIMMS dataset	ISLSCP II (Tucker et al., 2005, Hall <i>et al.</i> , 2006)	0.25 degrees	year 2002	Normalized difference vegetation index (NDVI)
Land-use	MODIS dataset	ISLSCP II (Friedl et al., 2010, Hall <i>et al.</i> , 2006)	0.25 degrees	year 2002	Land use fractions

Table 2. Fractal parameters and the resulting mean global slopes before and after applying the fractal method on the different DEMs; Increase of slope means the increase of the average global slope of a DEM after applying the fractal method; difference after scaling

$$= \frac{\theta_{scaled(DEM)} - \theta_{scaled(GTOPO30)}}{\theta_{scaled(GTOPO30)}} * 100; \text{ difference before scaling} = \frac{\theta_{(DEM)} - \theta_{(GTOPO30)}}{\theta_{(GTOPO30)}} * 100$$

DEM	resolution arc-minute	standard deviation of elevation m	mean D	mean $\alpha_{steepest}$	θ m m-1	θ_{scaled} m m-1	Increase of θ %	difference after scaling %	difference before scaling %
GTOPO30	0.5	570	1.32	0.99	0.023	0.059	61	0	0
ETOPO1	1	530	1.35	1.08	0.016	0.057	71.9	-3.4	-30.4
ETOPO2	2	549	1.37	1.17	0.011	0.055	80	-6.8	-52.2
ETOPO5	5	562	1.42	1.25	0.006	0.054	88.9	-8.5	-73.9

Table 3. Description of Köppen climate symbols and defining criteria (from Peel et al., 2007).

1st	2nd	3rd	Description	Criteria*
A			Tropical	$T_{cold} \geq 18$
	f		- Rainforest	$P_{dry} \geq 60$ Not (Af) & $P_{dry} \geq 100 - MAP/25$
	m		- Monsoon	MAP/25
	w		- Savannah	Not (Af) & $P_{dry} < 100 - MAP/25$
B			Arid	$MAP < 10 \times P_{threshold}$
	W		- Desert	$MAP < 5 \times P_{threshold}$
	S		- Steppe	$MAP \geq 5 \times P_{threshold}$
		h	▪ Hot	$MAT \geq 18$
	k	▪ Cold	$MAT < 18$	
C			Temperate	$T_{hot} > 10 \& T_{cold} < 18$
	s		- Dry Summer	$P_{sdry} < 40 \& P_{sdry} < P_{wwet}/3$
	w		- Dry Winter	$P_{wdry} < P_{swet}/10$
	f		- Without dry season	Not (Cs) or (Cw)
		a	▪ Hot Summer	$T_{hot} \geq 22$
		b	▪ Warm Summer	Not (a) & $T_{mon10} \geq 4$
		c	▪ Cold Summer	Not (a or b) & $1 \leq T_{mon10} < 4$
D			Cold	$T_{hot} > 10 \& T_{cold} \leq 0$
	s		- Dry Summer	$P_{sdry} < 40 \& P_{sdry} < P_{wwet}/3$
	w		- Dry Winter	$P_{wdry} < P_{swet}/10$
	f		- Without dry season	Not (Ds) or (Dw)
		a	▪ Hot Summer	$T_{hot} \geq 22$
		a	▪ Warm Summer	Not (a) & $T_{mon10} \geq 4$
		c	▪ Cold Summer	Not (a, b or d)
	d	▪ Very Cold Winter	Not (a or b) & $T_{cold} \leq -38$	
E			Polar	$T_{hot} < 10$
	T		- Tundra	$T_{hot} > 0$
	F		- Frost	$T_{hot} < -0$

* MAP = mean annual precipitation, MAT = mean annual temperature, T_{hot} = temperature of the hottest month, T_{cold} = temperature of the coldest month, T_{mon10} = number of months where the temperature is above 10, P_{dry} = precipitation of the driest month, P_{sdry} = precipitation of the driest month in summer, P_{wdry} = precipitation of the driest month in winter, P_{swet} = precipitation of the wettest month in summer, P_{wwet} = precipitation of the wettest month in winter, $P_{threshold}$ = varies according to the following rules (if 70% of MAP occurs in winter then $P_{threshold} = 2 \times MAT$, if 70% of MAP occurs in summer then $P_{threshold} = 2 \times MAT + 28$, otherwise $P_{threshold} = 2 \times MAT + 14$). Summer (winter) is defined as the warmer (cooler) six month period of ONDJFM and AMJJAS.

Table 4. Linear multiple regression equations for different climate zones, relating high resolution erosivity from the USA with one or more significant parameters: annual total mean precipitation (P), mean elevation (z) and the simple precipitation intensity index ($SDII$)

Climate zone	Explaining parameters	Regression function - optimal	R^2	Residual standard error
BWk	P, SDII	$R = 0.809 * P^{0.957} + 0.000189 * SDII^{6.285}$		
BSh	P, SDII	$\log R = -7.72 + 1.595 * \log P + 2.068 * \log SDII$	0.97	0.22
BSk	P, SDII, Z	$\log R = 0.0793 + 0.887 * \log P + 1.892 * \log SDII - 0.429 * \log Z$	0.89	0.35
Csb	P	$R = 98.35 + 0.000355 * P^{1.987}$		0.16
Cfa	P, SDII, Z	$\log R = 0.524 + 0.462 * \log P + 1.97 * \log SDII - 0.106 * \log Z$	0.89	0.11
Cfb	P, SDII	$\log R = 4.853 + 0.676 * \log P + 3.34 * \log SDII$	0.97	0.21
Dsa	Z, SDII	$\log R = 8.602 - 0.963 * \log SDII - 0.247 * \log Z$	0.51	0.05
Dsb	P	$\log R = 2.166 + 0.494 * \log P$	0.45	0.25
Dsc	SDII	$\log R = 6.236 - 0.869 * \log SDII$	0.51	0.02
Dwa	P	$\log R = -0.572 + 1.238 * \log P$	0.99	0.02
Dwb	P, SDII	$\log R = -1.7 + 0.788 * \log P + 1.824 * \log SDII$	0.98	0.02
Dfa	P, SDII	$\log R = -1.99 + 0.737 * \log P + 2.033 * \log SDII$	0.9	0.16
Dfb	P, SDII, Z	$\log R = -0.5 + 0.266 * \log P + 3.1 * \log SDII - 0.131 * \log Z$	0.89	0.32
Dfc	SDII	$\log R = -1.259 + 3.862 * \log SDII$	0.91	0.23
ET	P	$\log R = -3.945 + 1.54 * \log P$	0.14	0.42
EF+EFH	P	$\log R = 16.39 - 1.286 * \log P$	0.6	0.13

ETH	P, SDII	$\log R = 21.44 + 1.293 * \log P - 10.579 * \log SDII$	0.52	0.53
-----	---------	--	------	------

Table 5. Linear multiple regression equations for different climate zones for regions that have no data on the simple precipitation intensity index (*SDII*). The regression equations relate high resolution erosivity from the USA with the annual total mean precipitation (*P*) and/or the mean elevation (*z*)

Climate zone	Optimal regression function (when SDII is not available)	R ²	Residual standard error
BWk	Method Renard & Freimund (1994)		
BSh	$\log R = -8.164 + 2.455 * \log P$	0.86	0.5
BSk	$\log R = 5.52 + 1.33 * \log P - 0.977 * \log Z$	0.76	0.52
Cfa	$\log R = 3.378 + 0.852 * \log P - 0.191 * \log Z$	0.57	0.23
Cfb	$\log R = 5.267 + 0.839 * \log P - 0.635 * \log Z$	0.81	0.5
Dsa	$\log R = 7.49 - 0.0512 * \log P - 0.272 * \log Z$	0.48	0.06
Dsc	$\log R = 4.416 - 0.0594 * \log P$	0.015	0.03
Dwb	$\log R = 1.882 + 0.819 * \log P$	0.81	0.08
Dfa	$\log R = -2.396 + 1.5 * \log P$	0.65	0.29
Dfb	$\log R = 1.96 + 1.084 * \log P - 0.34 * \log Z$	0.74	0.48
Dfc	$\log R = -3.263 + 1.576 * \log P$	0.56	0.49
ETH	$\log R = -10.66 + 2.43 * \log P$	0.4	0.59

Table 6. Mean high resolution R values from the USA and Switzerland and mean modelled R values with uncertainty range for each addressed climate zone

climate	description	observed R mean	old method R mean	adjusted method R mean	Adjusted method uncertainty range
BWk	arid, desert, cold	284	533	291	158-495
BSh	arid, steppe, hot	2168	1356	2207	1723-2828
BSk	arid, steppe, cold	876	884	885	749-1046
Csb	temperate, dry warm summer	192	1136	192	133-292
Cfa	temperate, without dry season, hot summer	5550	5607	5437	4830-6123
Cfb	temperate, without dry season, warm summer	1984	5359	1971	1431-2715
Dsa	cold, dry hot summer	172	445	171	86-340
Dsb	cold, dry warm summer	175	896	168	151-187
Dsc	cold, dry cold summer	115	374	115	91-145
Dwa	cold, dry winter, hot summer	1549	1444	1551	1280-1879
Dwb	cold, dry winter, warm summer	1220	1418	1214	1057-1395
Dfa	cold, without dry season, hot summer	2572	2983	2582	2346-2843
Dfb	cold, without dry season, warm summer	1101	1798	1124	922-1371
Dfc	cold, without dry season, cold summer	483	701	483	423-552
ET	polar, tundra	1352	6257	1249	23-68088
EF+EFH	polar, frost + polar, frost, high elevation	1468	5469	1450	16-132001
ETH	polar, tundra, high elevation	945	5580	832	0-6314918

Table 7. Statistics of the comparison of high resolution erosivity from three regions to estimated erosivity from the Renard and Freimund method and the new regression equations

	Observed			Estimated – Renard & Freimund				Estimated – multiple linear regression					
	Range	Mean	Standard deviation	Range	Mean	Standard deviation	Correlation coefficient	Rank correlation coefficient	Range	Mean	Standard deviation	Correlation coefficient	Rank correlation coefficient
Switzerland	121-6500	1204	833	2335-10131	5798	1654	0.51	0.42	225-2572	1256	472	0.49	0.3
the USA (aggregated huc4)	105-4963	1271	1174	57-15183	1870	2088	0.51	0.68	60-15808	1691	2188	0.58	0.83
Ebro basin	40 - 4500	891	622	747 - 5910	1529	846	-	-	167 - 4993	836	701	-	-

Table 8. Comparison of the global erosion rates ($\text{t ha}^{-1} \text{y}^{-1}$) and percentiles between different versions of the RUSLE model

	mean	25th percentile	50th percentile	75th percentile	90th percentile
RUSLE unadjusted	5.1	0.2	0.8	2.8	8.6
RUSLE adjusted with S	11.1	0.3	1.2	4.3	15.7
RUSLE adjusted with R	3.6	0.1	0.6	1.9	6.3
RUSLE adjusted with S & R	7.3	0.2	0.8	3	10.9

Table 9. Statistics of the observed and modelled erosion rates from the unadjusted and adjusted versions of the RUSLE for the USA and Europe ($t\ ha^{-1}\ y^{-1}$)

Region	Source	Observations			Adjusted RUSLE			Unadjusted RUSLE		
		Range	Mean	Standard deviation	Range	Mean	Standard deviation	Range	Mean	Standard deviation
Europe (Aggregation country level) no small countries	Cerdan et al., 2010	0.1-2.6	0.9	0.7	0.1-7	2.3	2.1	0-14	2.8	3.6
the USA (Aggregation HUC4 level)	NRI database	0-11	1.7	2.1	0.2-21	1.7	2.5	0-14	1.9	2.3

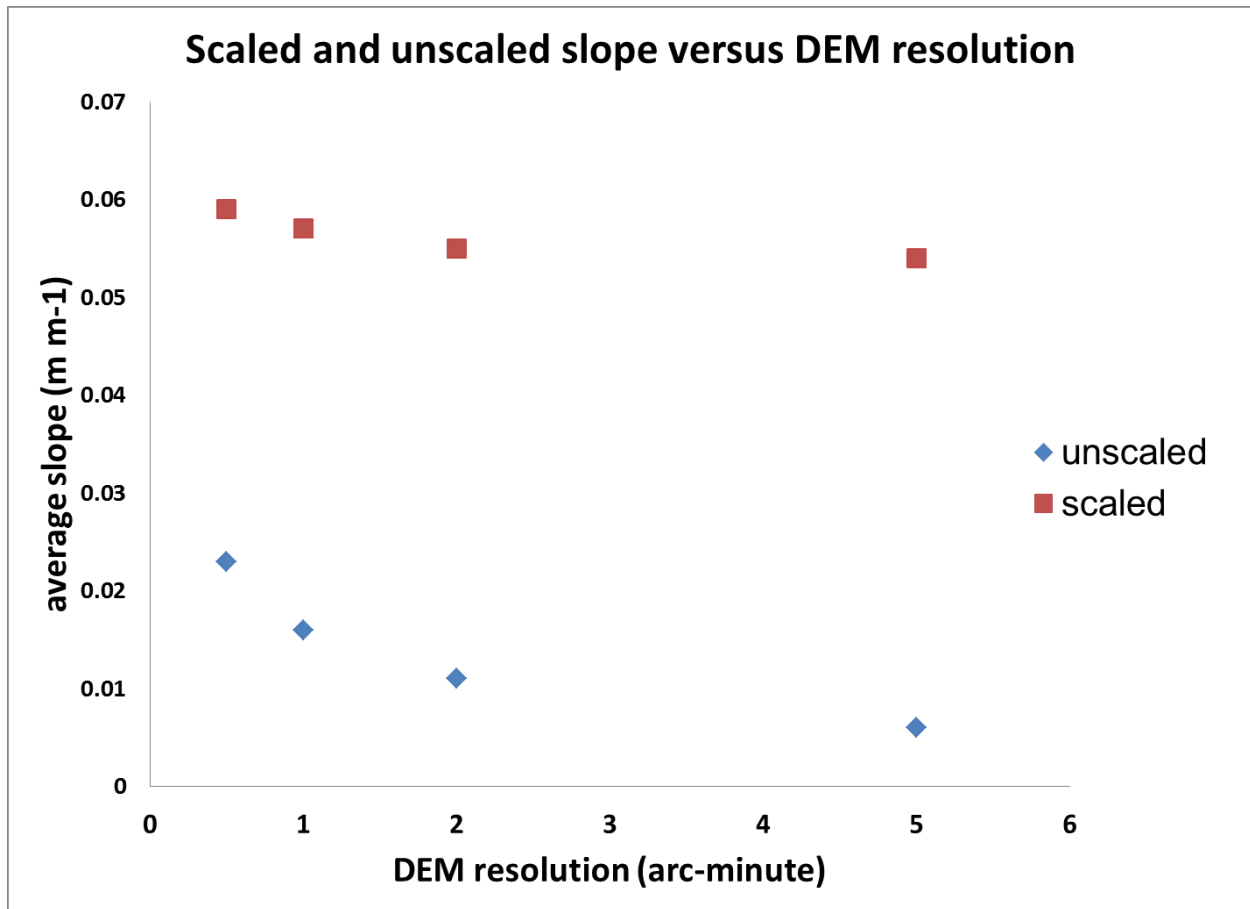
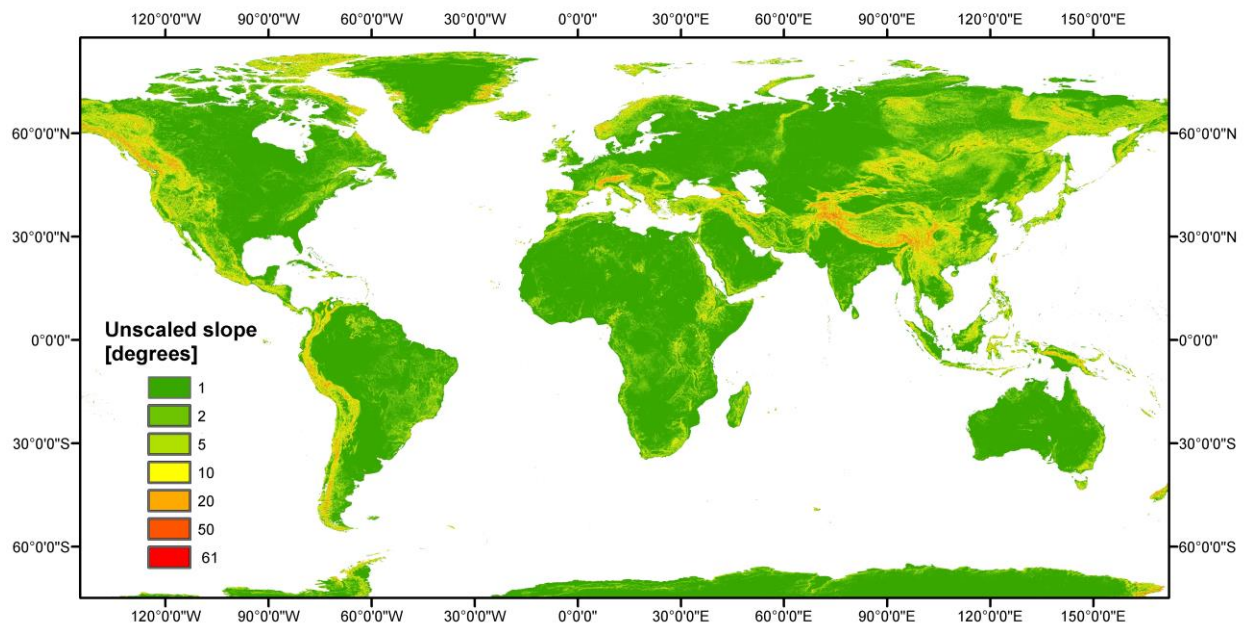


Figure 1. Global average unscaled slope estimated from different coarse resolution digital elevation models (DEMs) as function of their resolution (blue); and global average scaled slope from the same DEMs as function of their resolution (red).

(A)



(B)

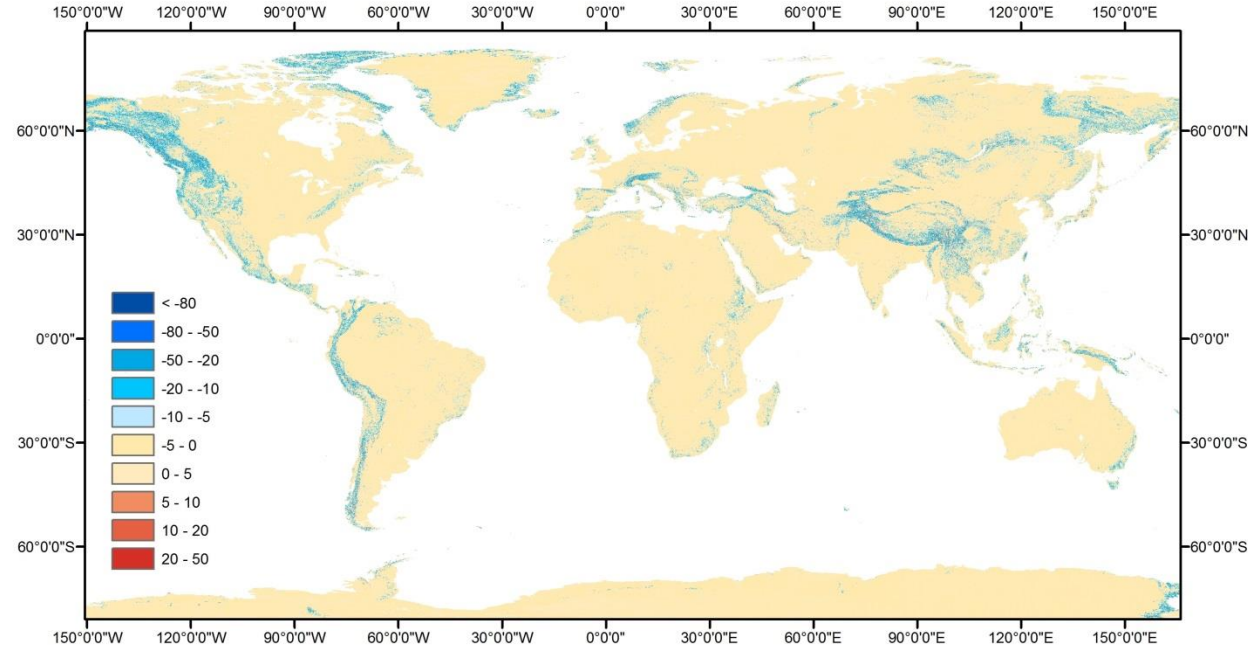


Figure 2. (A) A global map of the unscaled slope derived from the 30 arc-second DEM using a target resolution of 150m; (B) A global map showing the difference between the unscaled and scaled slopes (in degrees), where blue colours show an underestimation by the unscaled slope when compared to the scaled slope and reddish colours show an overestimation.

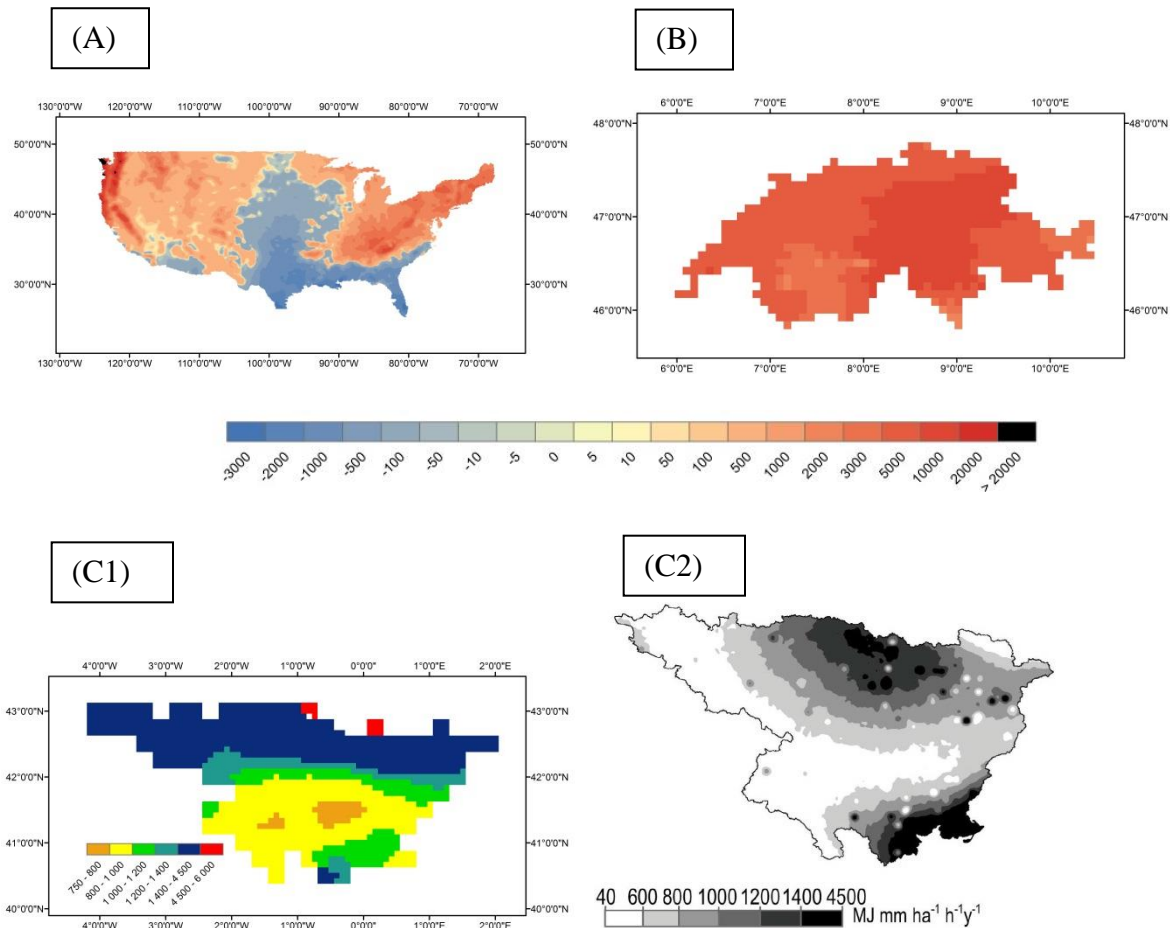


Figure 3. Spatial difference plots showing the difference between the high resolution erosivity and erosivity calculated with the method of Renard and Freimund for (A) the USA, (B) Switzerland and (C) the Ebro basin in Spain; In (A) and (B) the blue colours show an underestimation of the calculated erosivity when compared to the high resolution erosivity, while the red colours show an overestimation; the Ebro basin serves here as an independent validation

set and it has two graphs, (C1) a spatial plot of erosivity according to Renard and Freimund, and (C2) the high resolution erosivity from Angulo-Martinez et al. (2009); All values in the graphs are in $\text{MJ mm ha}^{-1} \text{h}^{-1} \text{y}^{-1}$

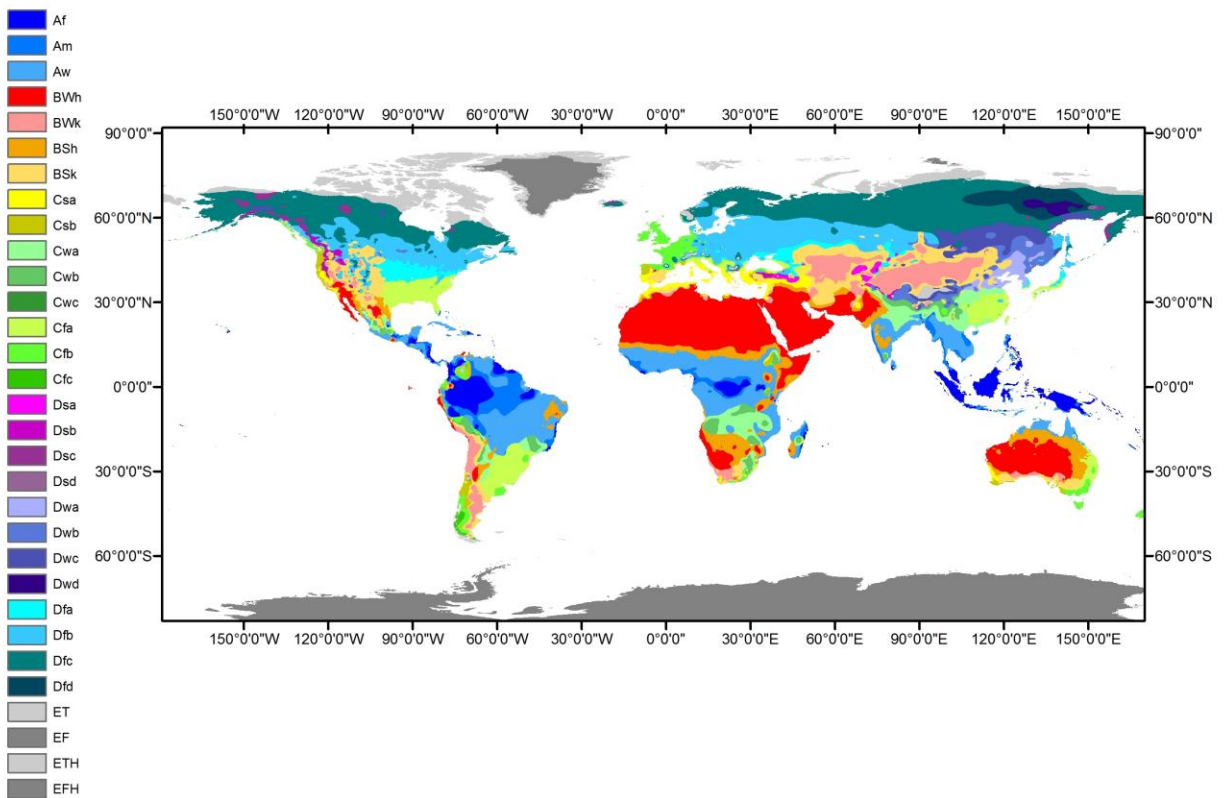
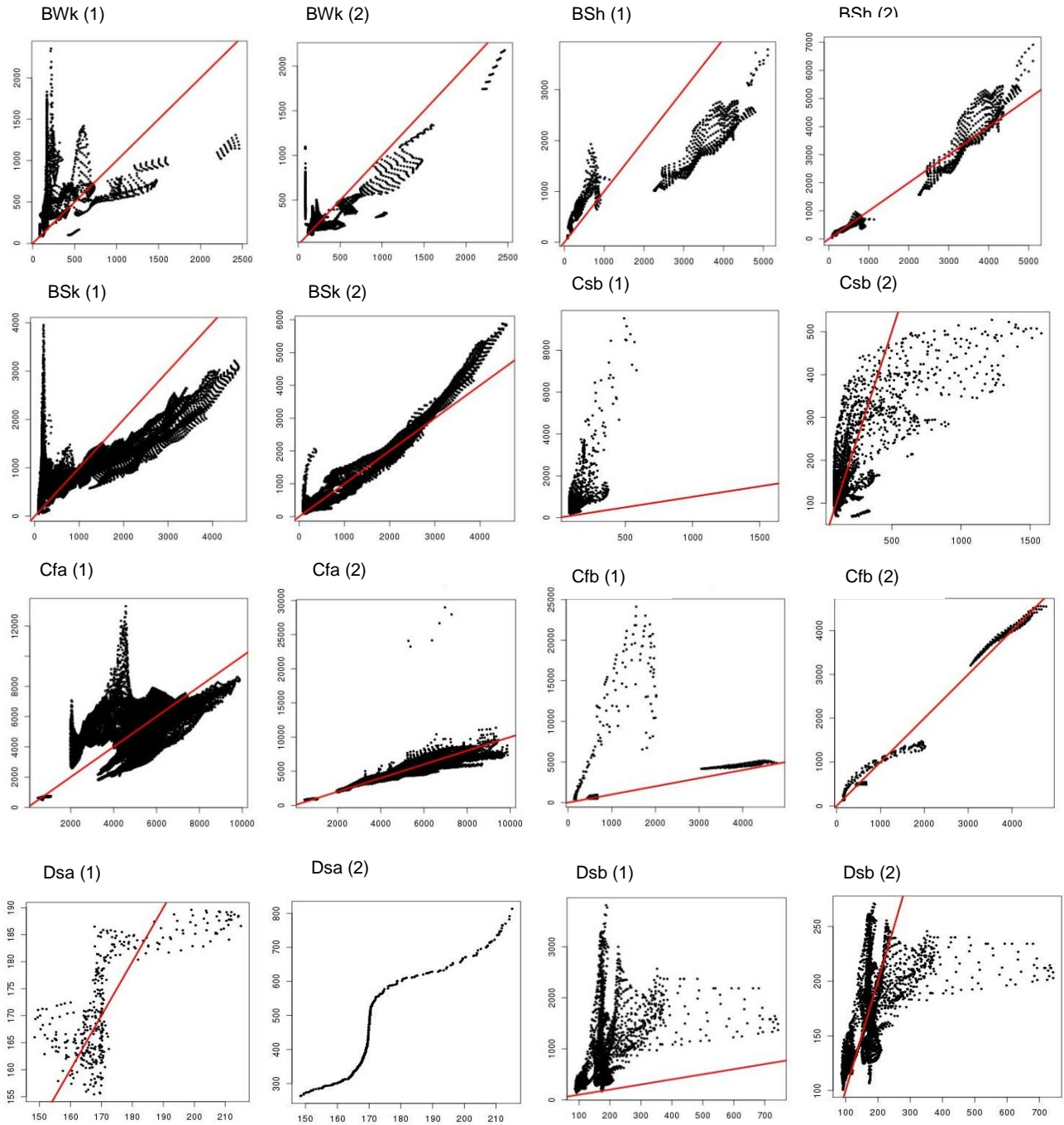
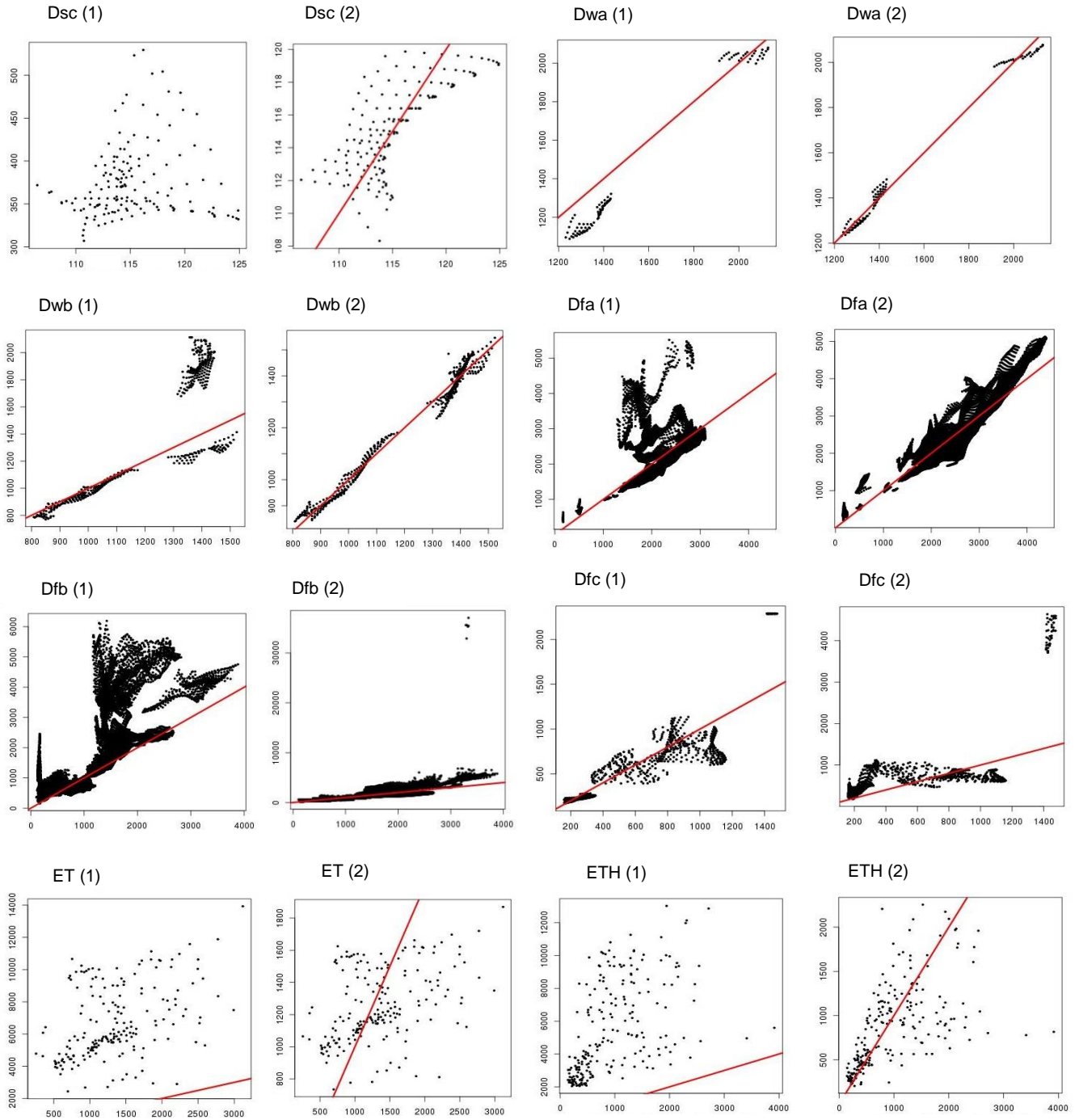


Figure 4. The Köppen-Geiger climate classification global map with resolution of 5 arc-minute (Peel et al., 2007)





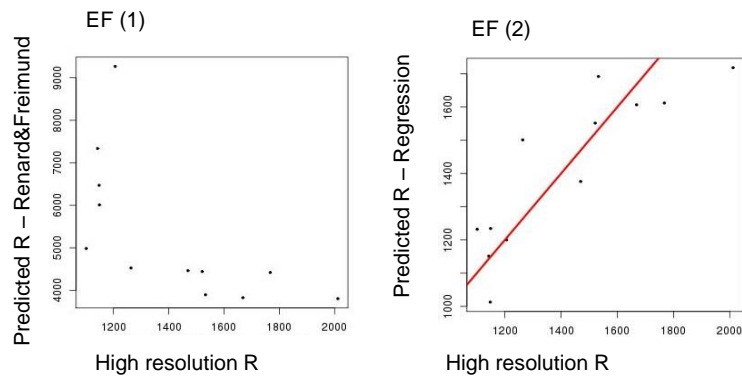


Figure 5. Comparison of high resolution erosivity data and predicted erosivity from (1) the Renard and Freimund method and (2) the new regression equations, for various climate zones; the red line is the 1 tot 1 line that always lies on the 45 degree diagonal, and does not appear in some graphs because predicted erosivity is overestimated; All values in the graphs are in MJ $\text{mm ha}^{-1} \text{h}^{-1} \text{y}^{-1}$

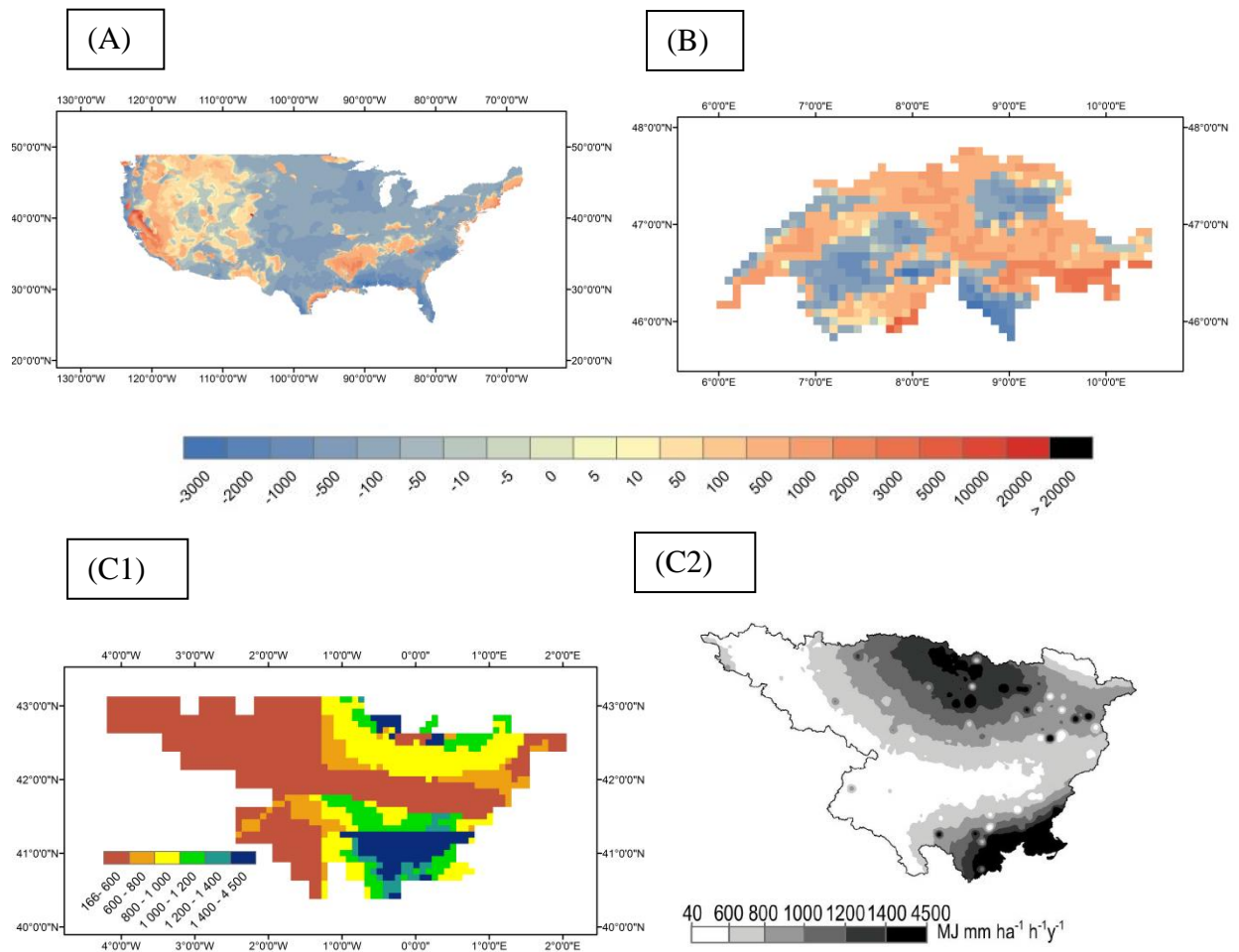


Figure 6. Spatial difference plots showing the difference between the high resolution rainfall erosivity and erosivity calculated with the new regression equations for (A) the USA, (B) Switzerland and (C) the Ebro basin in Spain; In (A) and (B) the blue colours show an underestimation of the calculated erosivity when compared to the high resolution erosivity, while the red colours show an overestimation; the Ebro basin serves here as an independent validation set and it has two graphs, (C1) a spatial plot of erosivity according to the new regression equations, and (C2) the high resolution erosivity from Angulo-Martinez et al. (2009); All values in the graphs are in $\text{MJ mm ha}^{-1} \text{h}^{-1} \text{y}^{-1}$; The Ebro basin is presented differently here when compared to the USA and Switzerland, due to the lack of the original erosivity data from Angulo-Martinez et al., 2009.

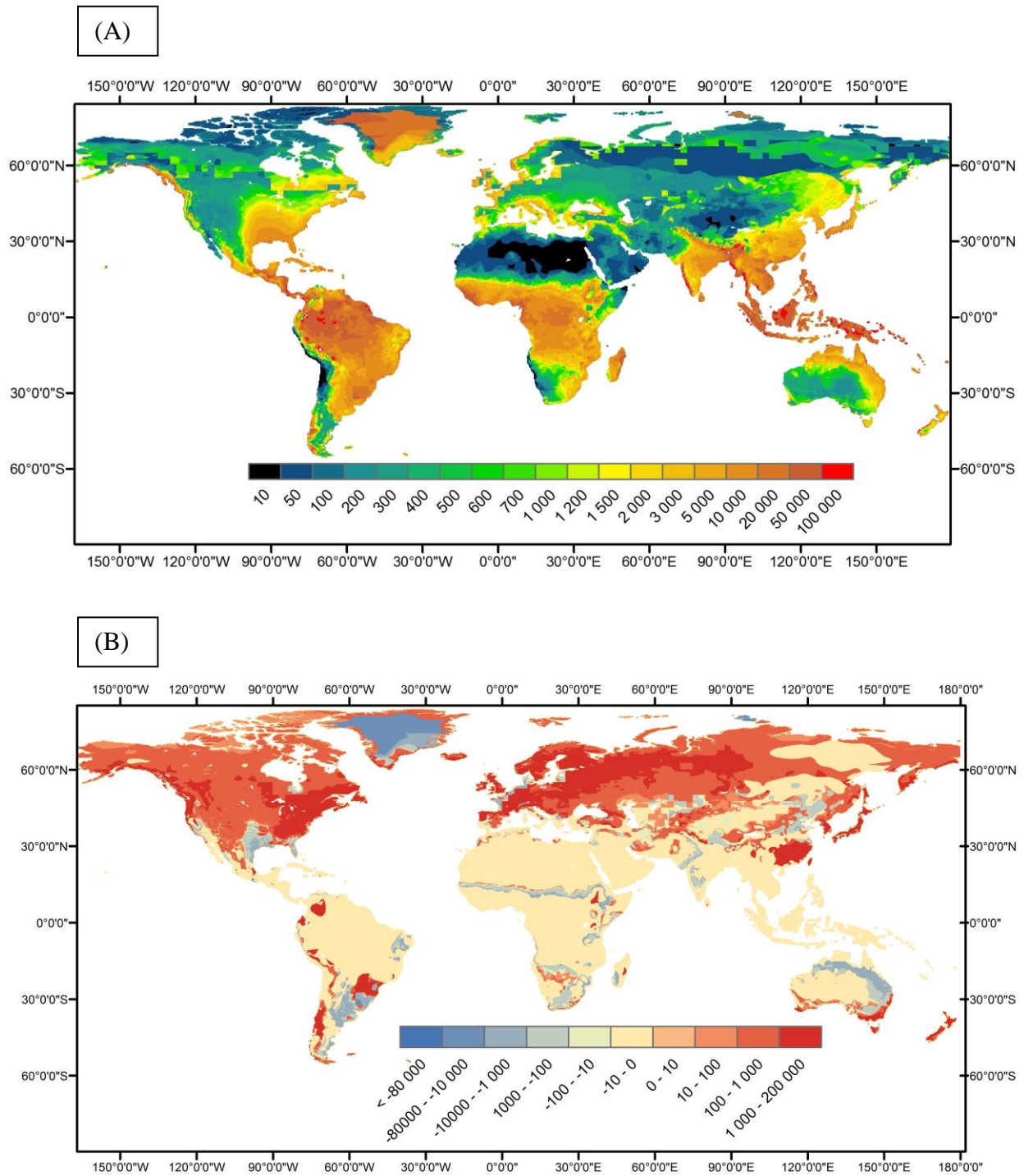
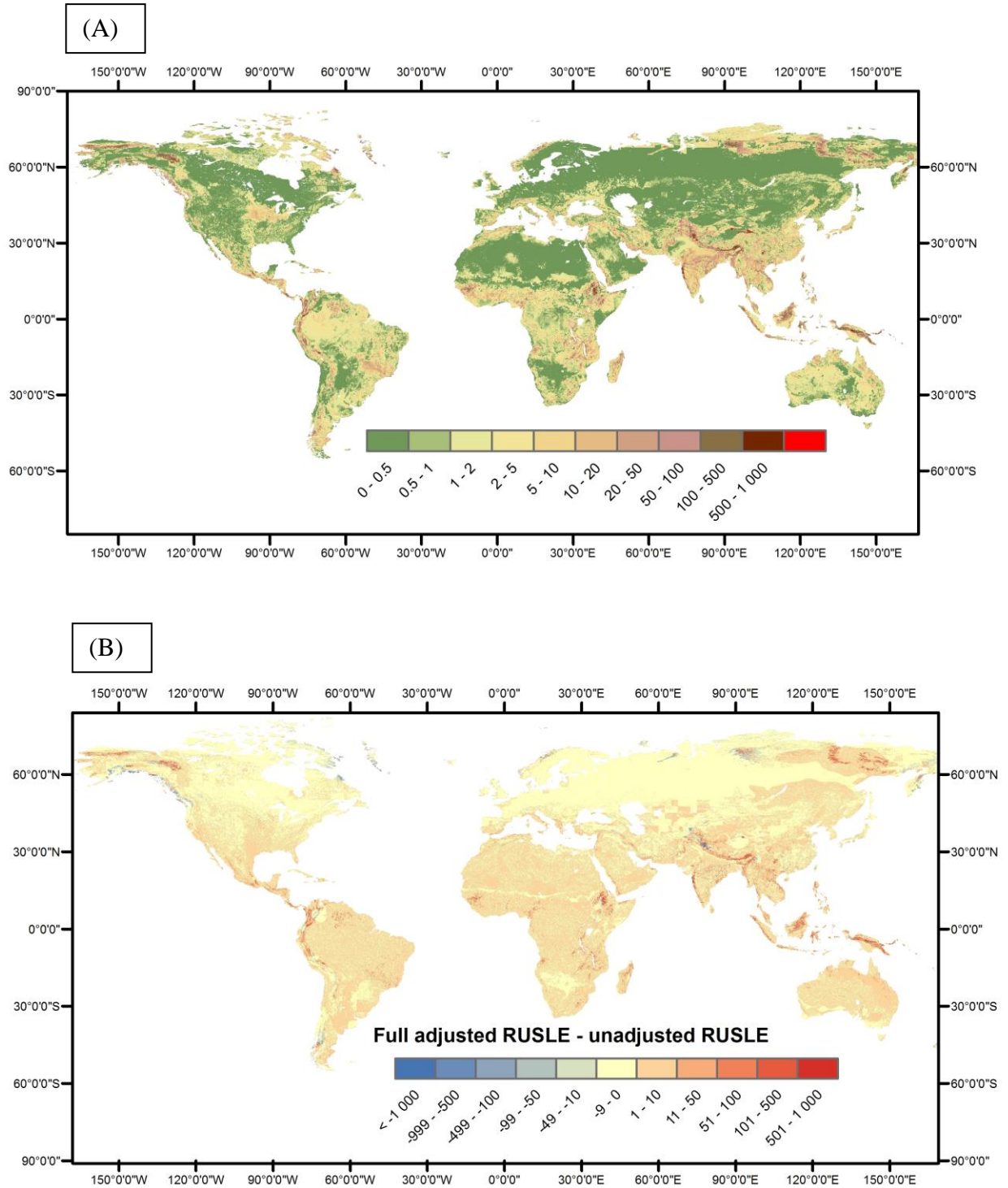


Figure 7. (A) Global distribution of the new modelled rainfall erosivity values according to the new regression equations; and (B) a difference map between erosivity calculated according to the method of Renard and Freimund and the new modelled erosivity values ($\text{MJ mm ha}^{-1} \text{ h}^{-1} \text{ y}^{-1}$),

where blue colours indicate lower erosivity values by Renard and Freimund, while redish colours indicate higher erosivity values; map resolution is 5 arc-minute



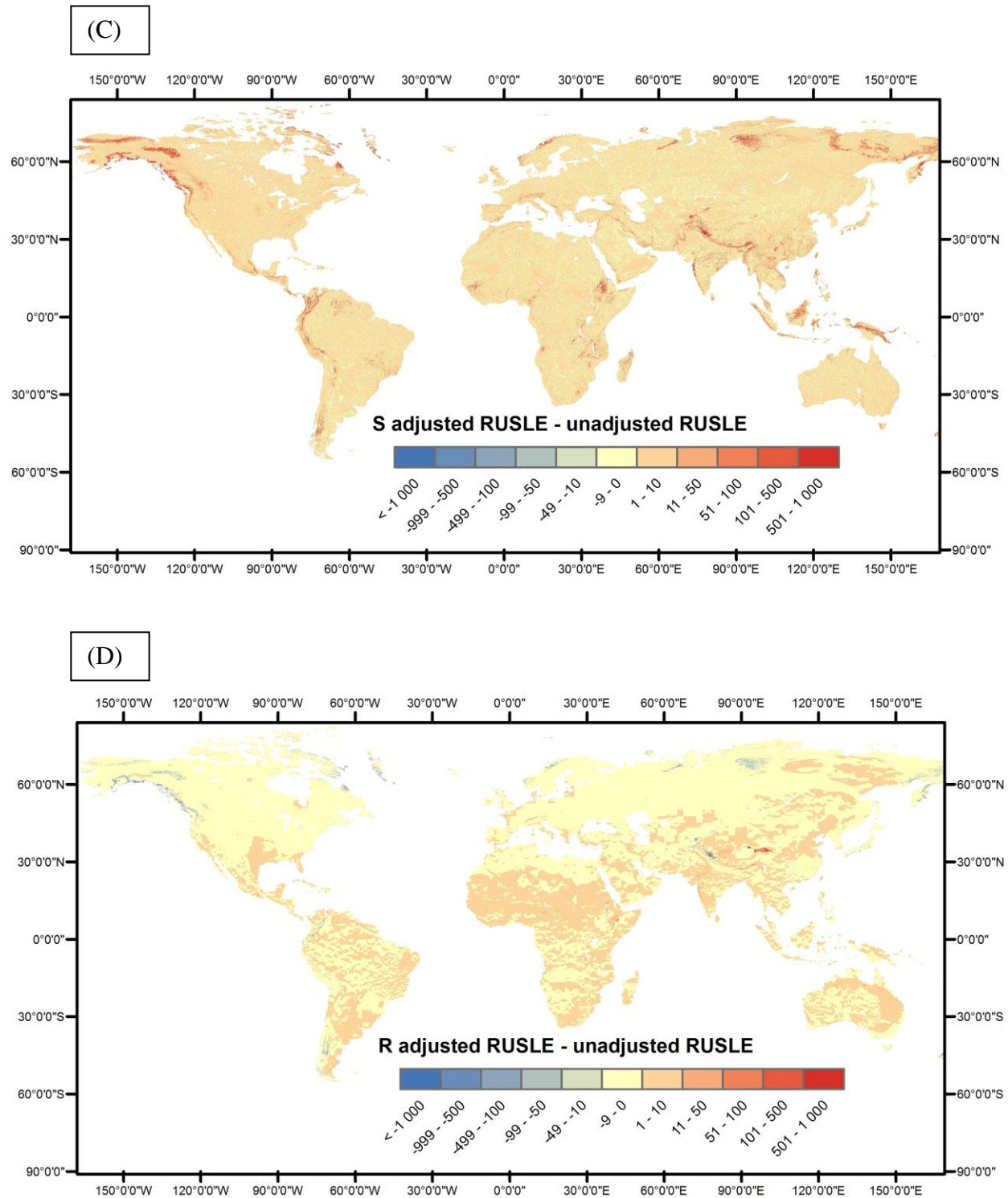
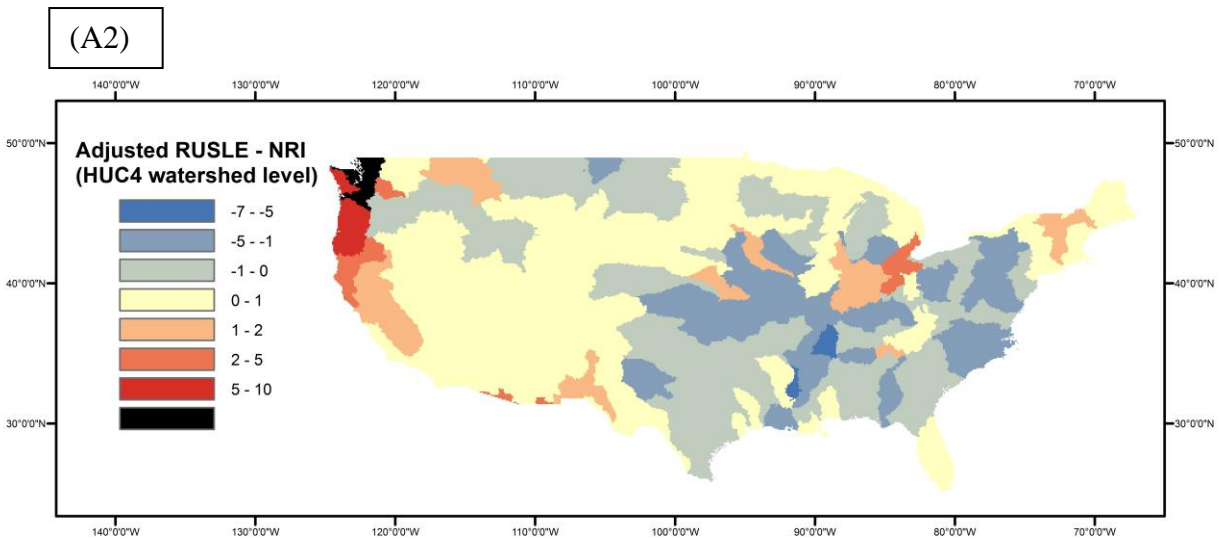
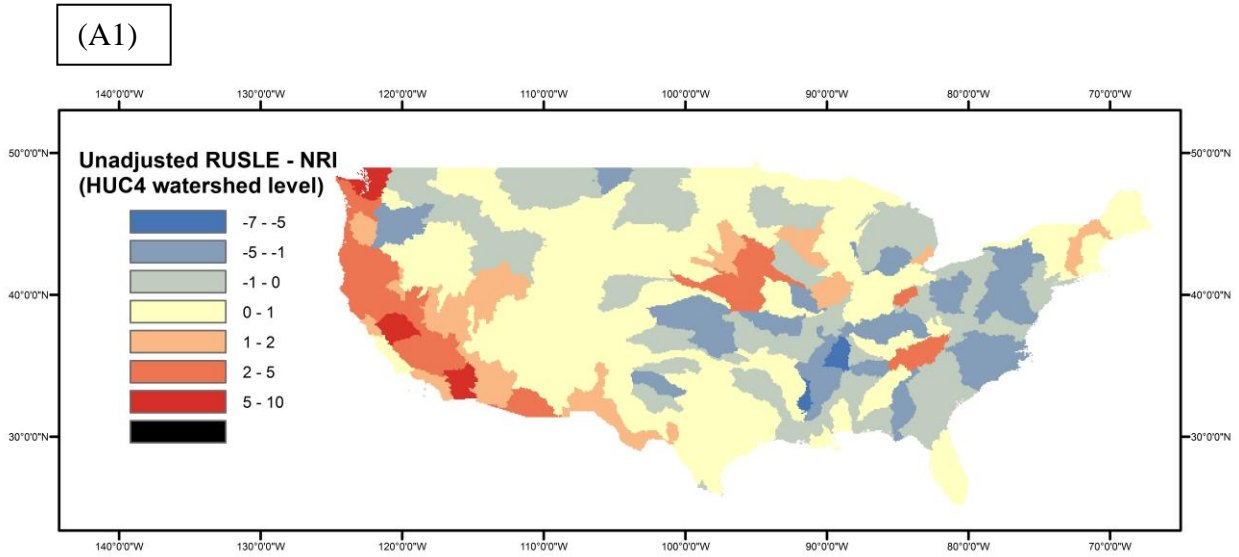


Figure 8. (A) Global yearly averaged erosion rates according to the fully adjusted RUSLE model; (B) a difference map between the fully adjusted and unadjusted RUSLE model; (C) a difference map between the adjusted S RUSLE and the unadjusted RUSLE model; (D) a difference map between the adjusted R RUSLE and the unadjusted RUSLE model; in figures

B,C and D the reddish colors show an overestimation of by the adjusted RUSLE model and yellow to bluish colors show an underestimation; resolution of all maps is 5 arc-minute and the units are in $t\ ha^{-1}\ y^{-1}$



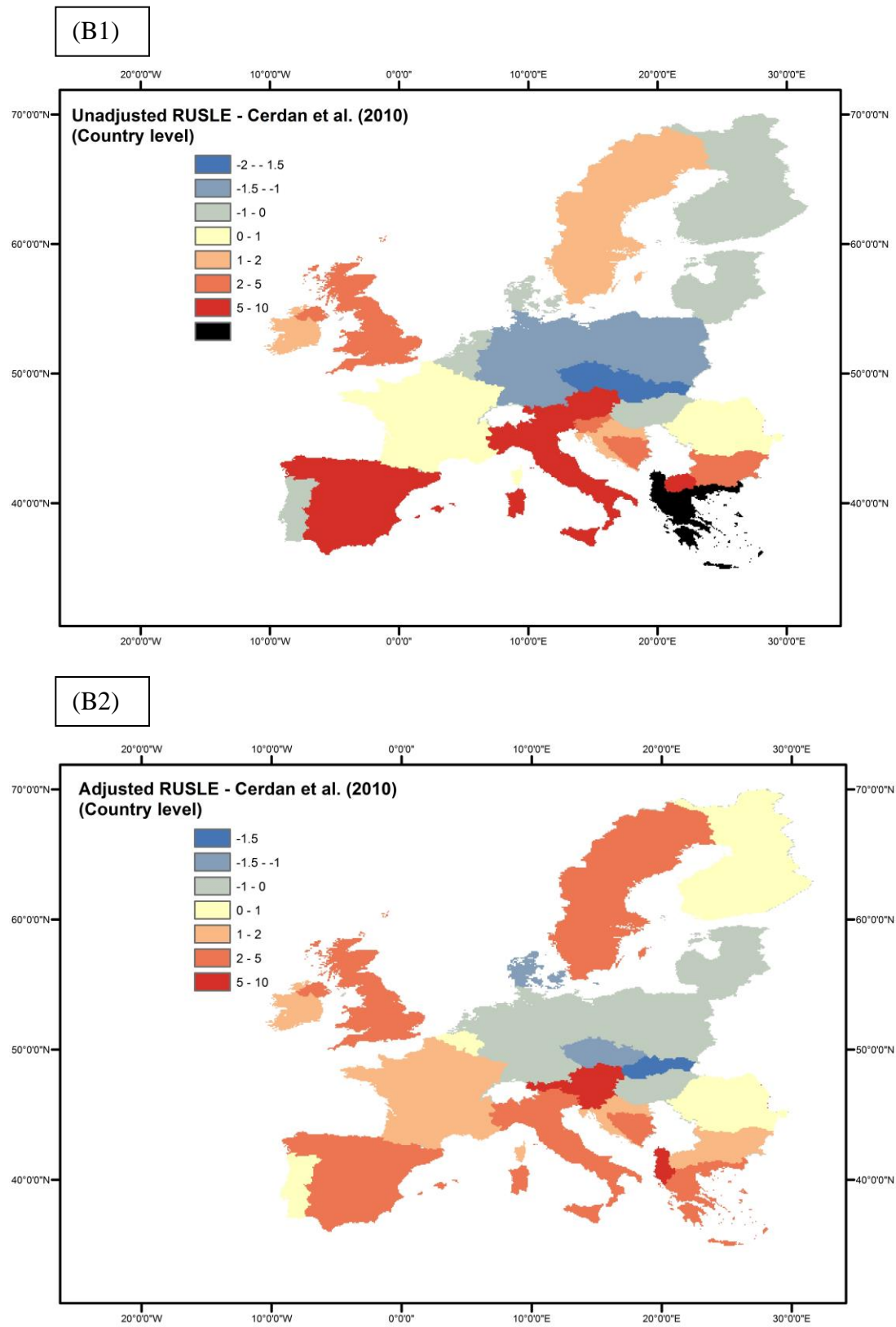


Figure 9. (A) Difference plots between soil erosion estimates from the NRI database for the USA and estimates of (A1) the unadjusted RUSLE model, and of (A2) the adjusted RUSLE model; all

aggregated at HUC4 watershed level; (B) Difference plots between soil erosion estimates from the database of Cerdan et al. (2010) for Europe and estimates of (B1) the unadjusted RUSLE model and of (B2) the adjusted RUSLE model; all aggregated at country level; reddish colors represent an overestimation (%) while the bluish represent an underestimation (%) compared to the erosion values from the databases; black color is an overestimation > 10%.